
Product Manifold Representations for Learning on Biological Pathways

Daniel McNeela^{1,2,3} Frederic Sala^{*1} Anthony Gitter^{*1,2,3}

Abstract

Machine learning models that embed graphs in non-Euclidean spaces have shown substantial benefits in a variety of contexts, but their application has not been studied extensively in the biological domain, particularly with respect to biological pathway graphs. Such graphs exhibit a variety of complex network structures, presenting challenges to existing embedding approaches. Learning high-quality embeddings for biological pathway graphs is important for researchers looking to understand the underpinnings of disease and train high-quality predictive models on these networks. In this work, we investigate the effects of embedding pathway graphs in non-Euclidean mixed-curvature spaces and compare against traditional Euclidean graph representation learning models. We then train a supervised model using the learned node embeddings to predict missing protein-protein interactions in pathway graphs. We find large reductions in distortion and boosts on in-distribution edge prediction performance as a result of using mixed-curvature embeddings and their corresponding graph neural network models. However, we find that mixed-curvature representations underperform existing baselines on out-of-distribution edge prediction performance suggesting that these representations may overfit to the training graph topology. We provide our Mixed-Curvature Product Graph Convolutional Network code at <https://github.com/mcneela/Mixed-Curvature-GCN> and our pathway analysis code at <https://github.com/mcneela/Mixed-Curvature-Pathways>.

1. Introduction

Machine learning methods for embedding graphs (Wu et al., 2021) enable learning on data ranging from social media networks, to proteins and molecules, to phylogenies and knowledge graphs. These embeddings then enable useful node classification and edge prediction models, which can perform tasks as diverse as predicting whether a molecule is active against a given drug target or whether two users are likely to share a preference for a given product.

While traditional graph learning methods employ Euclidean representations (Grover & Leskovec, 2016), it is known that for certain graphs Euclidean representations are unable to perfectly preserve graph structure, regardless of what algorithm is used (Bourgain, 1985). As a result, recent works have studied whether lower graph distortion can be achieved by embedding in non-Euclidean spaces, such as hyperbolic space (Sala et al., 2018). Generally speaking, lower distortion correlates with better downstream task performance.

The works of Gu et al. (2019) and Giovanni et al. (2022) have examined embeddings into mixed-curvature products of spaces and heterogeneous manifolds, respectively. By “mixed-curvature products of spaces”, we mean a Cartesian product of embedding spaces having constant positive, negative, or zero curvature. These correspond to the model spherical, hyperbolic, and Euclidean spaces, respectively (Lee, 2018). While these methods have been evaluated on standard graph benchmarking datasets, their hypotheses have not been validated for specialized graphs found in biological pathways and networks, which may have properties and topologies that differ from general graphs in other domains. The product space approach is appealing because deciding a priori which space to embed into can be challenging.

Biological pathways are graphs that encode cellular processes. Typically, the nodes in such graphs are entities such as genes, proteins, or metabolites, and the edges designate relationships between them. For example, an edge connecting nodes A and B might indicate that the presence of protein A controls the transcription of gene B. Pathways are an important object of study in network biology as they can be used to infer subcellular relationships and understand the mechanisms underlying disease.

Embedding biological pathways is difficult because no

^{*}Equal contribution ¹Department of Computer Sciences, University of Wisconsin-Madison, Madison, WI, USA ²Morgridge Institute for Research, Madison, WI, USA ³Department of Biostatistics and Medical Informatics, University of Wisconsin-Madison, Madison, WI, USA. Correspondence to: Anthony Gitter <gitter@biostat.wisc.edu>.

canonical methods exist. Pathways exhibit a high degree of complexity. Some, due to a lack of study, are sparse while others exhibit high inter-connectivity. Their complex network structures suggest that non-Euclidean representations might provide significant benefits. However, no systematic study of embedding methods applied to biological pathway graphs has been undertaken. Only Euclidean embedding methods have been applied to pathway graphs (M A Basher & Hallam, 2020; Pershad et al., 2020), and because pathway graphs differ from standard graphs used to benchmark non-Euclidean embedding models, it is unknown to what extent these models would work for pathway graphs.

In this work, we study non-Euclidean embeddings of biological pathway graphs and their performance relative to standard Euclidean embeddings.¹ We perform a large-scale test of a variety of embedding methods to pathway graphs taken from PathBank, Reactome, HumanCyc, the NCI Pathway Interaction Database, and KEGG and embed into a number of different combinations of spaces. For each pathway graph, we determine a best embedding space, as measured by the lowest graph distortion, and learn the node embeddings for that graph. Although biological pathway databases are of high quality, they are incomplete and only capture a fraction of the knowledge about the relevant biological processes (Hanspers et al., 2020). Therefore, we investigate the downstream performance of our graph embeddings by predicting potentially missing pathway edges. Instead of only predicting held out pathway edges, we also examine the considerably more challenging task of predicting protein-protein interactions (PPIs) from an independent database that may participate in the pathway. We find that mixed-curvature representations outperform, as measured by distortion, Euclidean representations in all cases. Furthermore, the positive impact of improved embeddings seems to generalize to downstream tasks such as edge prediction, where we find improvements in area under the receiver operating characteristic curve (AUROC) and average precision (AP) for held out in-distribution edges. However, for out-of-distribution STRING PPI edges, we find that the mixed-curvature representations underperform baselines, perhaps suggesting that these representations overfit to the in-distribution graph topology.

2. Background and Related Work

2.1. Non-Euclidean Embeddings and Machine Learning

Much of the research into non-Euclidean embeddings in machine learning originated in studies of graphs and networks, where they were originally used to embed concept ontologies. For example, Nickel & Kiela (2017) developed a method for embedding into the Poincaré model of hyper-

bolic space and used it to generate node embeddings for the WORDNET ontology. Sala et al. (2018) expanded on this work by determining the precision-dimensionality tradeoffs inherent in hyperbolic embeddings. Ganea et al. (2018) and Chami et al. (2019) then produced generalized Hyperbolic Neural Networks and Hyperbolic Graph Convolutional Networks (GCNs) to perform prediction directly in hyperbolic space on data of various types. Gu et al. (2019) extended graph representation learning to a Cartesian product of hyperbolic, spherical, and Euclidean spaces, while Giovanni et al. (2022) further generalized this to a product of manifolds of heterogeneous curvature. Our approach follows that of Gu et al. (2019). More recently, hyperbolic and non-Euclidean geometries have been applied to contrastive learning (Desai et al., 2023) and attention blocks (Tseng et al., 2023).

Hyperbolic modeling approaches have been applied to embed biological and chemical data exhibiting hierarchical structure. Many methods focus on drug discovery, specifically drug repurposing (Lau et al., 2023) or drug target prediction (Yue et al., 2023; Poleksic, 2023; Zahra et al., 2023; Pogány & Antal, 2024). The hierarchical relationships in the Gene Ontology make it appealing for learning hyperbolic representations of its terms and their associated genes (Kim et al., 2021; Li et al., 2023). In transcriptomics, methods have been developed to visualize and estimate the curvature of gene expression samples (Zhou & Sharpee, 2021), embed single-cell RNA-seq data (Klimovskaia et al., 2020; Ding & Regev, 2021), and model differential expression signatures (Pogány & Antal, 2023). Finally, embedding biological sequences has enabled visualizing members of a protein family (Susmelj et al., 2023) and Bayesian phylogenetic inference (Macaulay et al., 2023).

2.2. Pathway Graphs and Embeddings

Pathway graphs have been well-studied from a biological perspective, but embedding them to facilitate downstream prediction tasks is relatively new. For example, M A Basher & Hallam (2020) developed a method called pathway2vec, which combines five different Euclidean embedding methods to learn embeddings of biological pathways. Similarly, Pershad et al. (2020) used node2vec to generate embeddings of PPI networks and used the resulting embeddings as one component of a method to predict response to psychiatric drugs. Pathway embeddings are a crucial input to models that operate on pathway network structures to make predictions. Euclidean GCNs have been broadly applied to biological pathways to predict cancer subtypes (Lee et al., 2020; Hayakawa et al., 2022), synthetic lethality (Lai et al., 2021), PPIs (Pham & Dang, 2021), cancer survival (Liang et al., 2022), textual pathway descriptions (Yang et al., 2022), and subcellular localization (Magnano & Gitter, 2023). However, there has been no systematic study

¹This work extends our workshop paper McNeela et al. (2023).

investigating the use of non-Euclidean and mixed-curvature embedding models for pathway graphs.

2.3. PPI Prediction

PPIs can be predicted based on combinations of proteins' sequence, expression, functional, evolutionary, or 3D structural features (Durham et al., 2023). One PPI prediction formulation is as an edge or link prediction task in a network of known PPIs (Li et al., 2022). This can be accomplished using features from the original graph or by learning node embeddings as features for the edge prediction task. For example, Feng et al. (2020) predict signaling cascades from PPI graphs by integrating transcriptomics and copy-number data into a GCN. Jiang et al. (2020) use graph embeddings to predict links that indicate an enzymatic reaction between pairs of molecules from the KEGG database. Finally, Zhang & Kabuka (2019) and Liu et al. (2020) leverage a combination of sequence and network information to predict PPIs.

3. Methods

3.1. Data Processing

We downloaded five pathway datasets from Pathway Commons (Rodchenkov et al., 2020) v12, namely, PathBank (Wishart et al., 2020), Reactome (Gillespie et al., 2022), HumanCyc (Romero et al., 2004), KEGG (Kanehisa et al., 2012), and the NCI Pathway Interaction Database (Schaefer et al., 2009). We used the `.txt` files containing interaction participants, edge types, and associated metadata. For each pathway in each dataset, we created a NetworkX (Hagberg et al., 2008) graph object and ignored Pathway Commons edge types, treating each edge as undirected with no additional annotations. We then generated edge lists for the undirected graphs and learned embeddings using the mixed-curvature embedding Python library (Gu et al., 2019). All subsequent experiments were performed only for those pathway graphs for which a unique "best" embedding space could be determined, defined as the space exhibiting minimum distortion. Those pathways which did not exhibit a unique embedding space of minimum distortion were discarded as there exists no canonical way to select a representative product space to compare embedding and edge prediction methods against. We also discarded one pathway from the Reactome dataset having 36,293 edges because its runtime on the edge prediction task was prohibitive and it is an extreme outlier in terms of pathway size (Table 1).

For edge prediction, we downloaded Homo sapiens PPIs from STRING v12.0 (Szkarczyk et al., 2023). In STRING, PPIs are listed as pairs of ENSEMBL protein identifiers. For each gene or protein node name in the given pathway dataset, we map it to its UniProt SwissProt identifier using the *My-*

Gene API (Xin et al., 2016). For each ENSEMBL protein identifier, we map it to the `Ensembl_HGNC_uniprot_id` listed in the STRING aliases file. We then iterate over all STRING PPI edges. For each pathway, if there exists a STRING PPI corresponding to two UniProt identifiers in the given pathway, we add an edge to the potential test set for that graph. We only included STRING edges with experimental evidence and discarded all edges with a score of less than 500 out of 1000. This yields a dataset of reasonable size for edge prediction, although the score used to filter edges can be tuned. Filtering using higher experimental evidence scores would likely yield less false positives in the list of candidate edges for each pathway graph; however, the relationship here is not strictly linear.

3.2. Learning Embeddings

We adopt the notation $\mathbb{S}_C^{s_i}$ for the spherical space having constant positive curvature C and dimension s_i , $\mathbb{H}_C^{h_j}$ for the hyperbolic space having constant negative curvature $-C$ and dimension h_j , and \mathbb{E}^{e_k} for the Euclidean space having zero curvature and dimension e_k . Given a collection of spherical, hyperbolic, and Euclidean spaces, each having an associated dimension and curvature, we write their Cartesian product space as

$$\mathcal{P} = \prod_{i=1}^m \mathbb{S}_{C_i}^{s_i} \times \prod_{j=1}^n \mathbb{H}_{C_{m+j}}^{h_j} \times \prod_{k=1}^p \mathbb{E}^{e_k}, \quad (1)$$

Here the product space \mathcal{P} consists of $m + n + p$ spaces and has total dimension $\sum_i s_i + \sum_j h_j + \sum_k e_k$. Following Gu et al. (2019), we call each individual $\mathbb{S}^{s_i}, \mathbb{H}^{h_i}, \mathbb{E}^{e_i}$ a *component* and the decomposition of the product space into components as in Eq. 1 the *signature* of the space.

We learn an embedding function $f : \mathcal{G} \rightarrow \mathcal{P}$ where \mathcal{G} is the space of pathway graphs and \mathcal{P} is a product manifold with a fixed, predefined signature. For embedding node u of a graph G on a product manifold \mathcal{P} having k th hyperbolic component $\mathbb{H}_{C_j}^{h_j}$ with curvature $-C_j$, we randomly initialize $f^k(u) = (p_0, p_1, \dots, p_{h_j})$ to a point on the hyperbolic manifold, parameterized using the *hyperboloid model*, i.e.

$$-p_0^2 + p_1^2 + \dots + p_{h_j}^2 = -C_j, \quad (2)$$

Similarly, for the l th spherical component with curvature C_i , we randomly initialize $f^l(u) = (p_0, p_1, \dots, p_{s_i})$ lying on the sphere

$$p_0^2 + p_1^2 + \dots + p_{s_i}^2 = C_i \quad (3)$$

and for the m th Euclidean component, we randomly initialize $f^m(u) = (p_1 + \dots, p_{e_k})$. For the Euclidean components, f is unconstrained. For the hyperbolic and spherical components, we require one extra dimension because we embed hyperbolic and spherical spaces of dimension n in \mathbb{R}^{n+1} . Squared distances in the product space decompose as sums

	PathBank	Reactome	KEGG	HumanCyc	NCI
Number of graphs	875	1723	82	242	212
Number of graphs with single best space	411	884	47	210	144
Number of graphs with multiple best spaces	464	839	35	32	68
Mean number of nodes	63.23	54.36	159.73	104.83	100.95
Mean number of edges	283.56	1091.79	657.39	289.62	531.98
Median number of nodes	53	24	152	73	73
Median number of edges	162	65	532	133	194

Table 1: General statistics summarizing the five pathway databases.

of squared distances in the component spaces (Lee, 2018), i.e.

$$d_{\mathcal{P}}(u, v)^2 = \sum_i d_{M_i}(\pi_i(u), \pi_i(v))^2 \quad (4)$$

for $u, v \in \mathcal{P}$, where π_i denotes projection onto the i th component. The learning of f takes place via optimization of the following loss function

$$\mathcal{L}(f) = \sum_{1 \leq u < v \leq n} \left| \left(\frac{d_{\mathcal{P}}(f(u), f(v))}{d_G(u, v)} \right)^2 - 1 \right| \quad (5)$$

where $d_G(u, v)$ denotes the graph distance between nodes u and v , defined as the length of the shortest path connecting them in G , and $d_{\mathcal{P}}(f(u), f(v))$ denotes the product manifold geodesic distance between the learned embeddings for nodes u and v . To learn the embedding function, we initially randomize the embeddings for all nodes, then train f so as to minimize \mathcal{L} using the Riemannian stochastic gradient descent optimization algorithm (Bonnabel, 2013), which extends stochastic gradient descent to arbitrary Riemannian manifolds.

The main metric used to evaluate our embeddings is the average graph distance *distortion*. We define the distortion \mathcal{D} of a learned embedding f relative to a graph $G = (V, E)$ to be

$$\mathcal{D}(f) = \frac{1}{|V|^2} \sum_{u, v \in V, u \neq v} \frac{|d_{\mathcal{P}}(f(u), f(v)) - d_G(u, v)|}{d_G(u, v)}$$

3.3. Hyperparameters

We create 252 embeddings for each pathway graph corresponding to different combinations of the number of hyperbolic, spherical, and Euclidean spaces; the learning rate; and the dimensionalities of each space (Appendix). We test having different numbers of components of each space, where the number of components of each type ranges from 0 to 3. We also constrain the total dimensionality of all spaces to sum to 100. This is to keep the comparison across different combinations fair by ensuring they each have the same representational capacity as governed by the number of dimensions.

3.4. Mixed-Curvature Product GCN

Similar to Bachmann et al. (2020), we extend the Hyperbolic GCN of Chami et al. (2019) to products of constant curvature manifolds. The following facts of Riemannian geometry allow us to extend GCNs from single manifolds to product manifolds.

Definition 3.1. Given Riemannian manifolds, $(M_1, g_1), \dots, (M_n, g_n)$, we can construct a *Riemannian product manifold* $(M_1 \times M_2 \times \dots \times M_n, g)$ with the *product metric*, $g = g_1 \oplus \dots \oplus g_n$, where the distance decomposes as

$$d_M(x, y)^2 = d_{M_1}(x_1, y_1)^2 + \dots + d_{M_n}(x_n, y_n)^2$$

for any $x = (x_1, \dots, x_n), y = (y_1, \dots, y_n) \in M$.

Thus, operations in the tangent spaces, $T_p M$, of the product manifold M decompose as direct sums of operations over the constituent tangent spaces $T_{p_i} M_i$, where $M = M_1 \times \dots \times M_n$ and $p = (p_1, \dots, p_n)$.

On each pathway graph for which we perform edge prediction, we match the signature of the product manifold in the GCN to the one used to learn the pathway embedding. The operations in the Product GCN are defined analogously to the ones in the hyperbolic GCN paper (Chami et al., 2019). Briefly put, pathway nodes are represented as a Cartesian product of points on some combination of components of \mathbb{H}^n , \mathbb{S}^n , and \mathbb{E}^n manifolds. At each layer in the Product GCN, the points are projected into a tangent space to the manifold via the log map of the product space and a GCN operates in this Euclidean tangent space using the standard message-passing updates. The points are then projected back onto the manifold after the layer operation via the product space exp map. Both the log map and the exp map decompose as sums over the constituent manifolds in the product space. The same procedure is used for attention and activation layers, with projection into the tangent space, followed by a standard layer operation, followed by projection back onto the manifold. For spherical (S) and hyperbolic

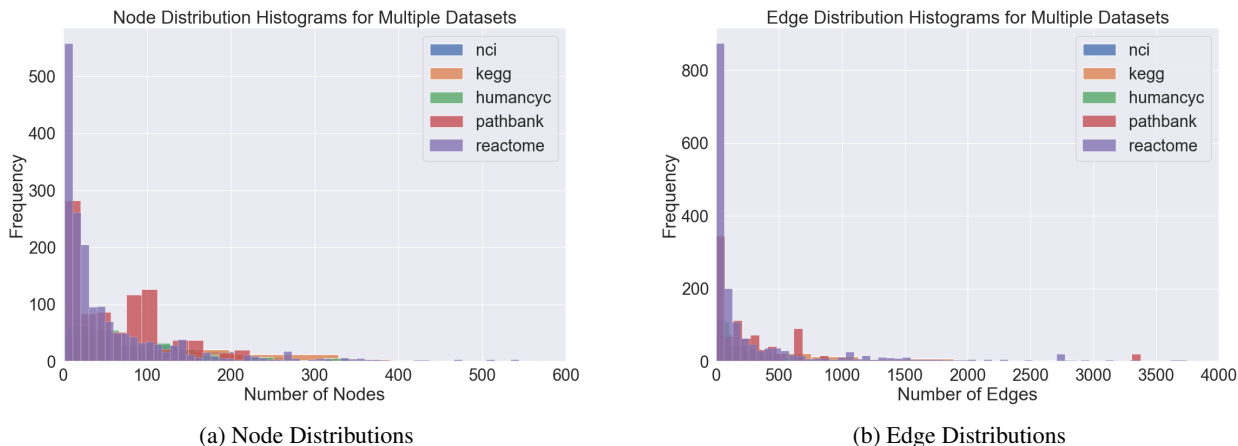


Figure 1. Histograms of node and edge distributions for the pathway databases studied. A few outliers were excluded.

(H) manifolds having curvatures C and $-C$, respectively, the exp and log maps are defined as follows:

$$\begin{aligned} \text{(S)} \quad \exp_{\mathbf{x}}^C(\mathbf{v}) &= \cos\left(\frac{\|\mathbf{v}\|}{\sqrt{C}}\right) \mathbf{x} + C \sin\left(\frac{\|\mathbf{v}\|}{\sqrt{C}}\right) \frac{\mathbf{v}}{\|\mathbf{v}\|} \\ \text{(H)} \quad \exp_{\mathbf{x}}^C(\mathbf{v}) &= \cosh\left(\frac{\|\mathbf{v}\|}{\sqrt{C}}\right) \mathbf{x} + \sqrt{C} \sinh\left(\frac{\|\mathbf{v}\|}{\sqrt{C}}\right) \frac{\mathbf{v}}{\|\mathbf{v}\|}, \\ \text{(S)} \quad \log_{\mathbf{x}}^C(\mathbf{y}) &= \cos^{-1}(\langle \mathbf{x}, \mathbf{y} \rangle_C) \frac{\mathbf{y} - \mathbf{x} - \langle \mathbf{x}, \mathbf{y} - \mathbf{x} \rangle_C \mathbf{x}}{\|\mathbf{y} - \mathbf{x} - \langle \mathbf{x}, \mathbf{y} - \mathbf{x} \rangle_C \mathbf{x}\|} \\ \text{(H)} \quad \log_{\mathbf{x}}^C(\mathbf{y}) &= \sqrt{C} \operatorname{arcosh}(-\langle \mathbf{x}, \mathbf{y} \rangle / C) \frac{\mathbf{y} + \frac{1}{C} \langle \mathbf{x}, \mathbf{y} \rangle \mathbf{x}}{\|\mathbf{y} + \frac{1}{C} \langle \mathbf{x}, \mathbf{y} \rangle \mathbf{x}\|} \end{aligned}$$

The Product GCN is trained using the Riemannian Adam optimization algorithm (Becigneul & Ganeva, 2019) on the edge prediction task described in Section 4.2.

4. Results

4.1. Pathway Embeddings

We first summarize each of the pathway databases in Table 1 and provide node and edge histograms in Figure 1. There exist uniquely beneficial product spaces, as measured by distortion, for only roughly half of the pathways. Most pathways are small by graph machine learning standards with the majority having less than 100 nodes and less than 200 edges. Thus, pathways exhibit a unique opportunity to study the effects of popular graph learning techniques, including GCNs, on small graphs, as most graph machine learning benchmarks possess thousands, or even millions and billions, of nodes and edges.

Next, for each pathway graph, we determine the best combi-

nation of hyperbolic, Euclidean, and spherical components as determined by lowest distortion. Figure 2(a) demonstrates the reductions in distortion gained from learning the non-Euclidean embeddings over all graphs in each of the five pathway datasets we studied. The red diagonal indicates the position at which the distortions of the Euclidean embeddings and mixed-curvature product embeddings would be equal. Points lying below this line indicate graphs for which a product representation yielded a reduction in distortion over a Euclidean representation. Because a fully Euclidean embedding is a special case of the mixed-curvature product embedding, the best mixed-curvature product embedding should always have better distortion than the best Euclidean embedding. The question is whether the improvement is marginal or substantial on biological pathways. We observe that mixed-curvature product spaces provide marked reductions in distortion relative to the standard Euclidean embedding, with many graphs achieving a greater than 50% reduction in distortion.

We further compare our mixed-curvature embeddings against two common graph embedding baselines. The first is node2vec (Grover & Leskovec, 2016), a popular graph embedding method which uses an algorithm analogous to word2vec (Mikolov et al., 2013) trained on random walks taken from the graph. We also compare against a standard embedding method formed by taking eigenvectors of the graph Laplacian matrix (Bonald, 2019). For both methods, we embed the pathway graphs from all datasets and compute distortions for each pathway embedding in each dataset. Because node2vec and the graph Laplacian embedding do not directly minimize distortion in their loss functions, they can arbitrarily scale embedding vectors, causing them to perform poorly on a naive calculation of the distortion metric. Therefore, we perform a scaling optimization for the node2vec and graph Laplacian embeddings, finding for each

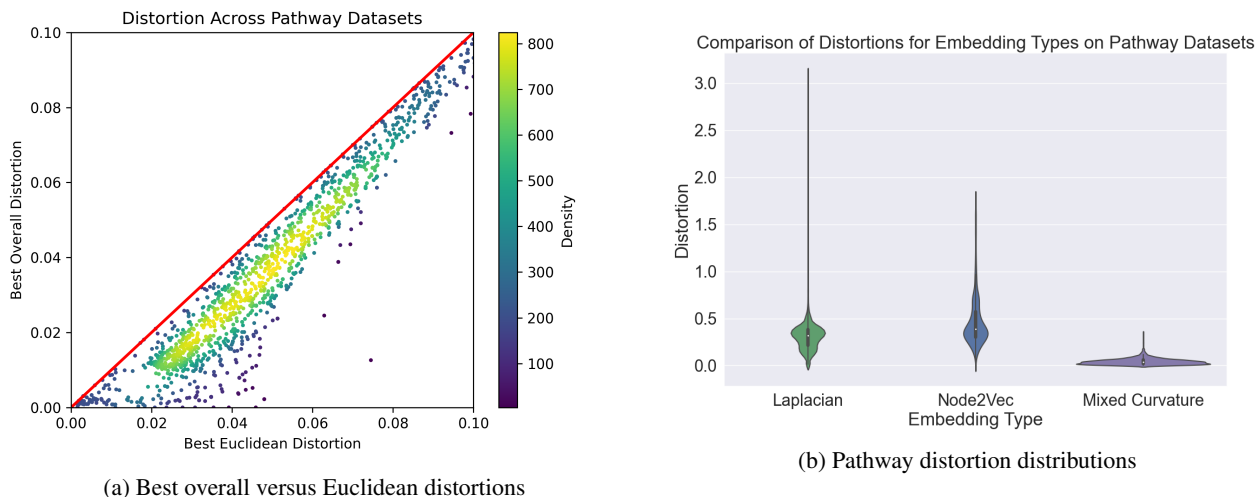


Figure 2. Best overall mixed-curvature versus best Euclidean distortions across all pathway datasets (a). See Figure 4 for individual pathway datasets. Distortions across all datasets for the graph Laplacian, node2vec, and mixed-curvature embedding methods (b).

dataset and embedding type the constant c which minimizes the below objective

$$\min_{c \in \mathbb{R}^+} \sum_{i < j} \left(\frac{c \cdot d(x_i, x_j)}{d_G(n_i, n_j)} - 1 \right)$$

where $d(x_i, x_j)$ is the distance between the embeddings of nodes i and j , and $d_G(n_i, n_j)$ is the shortest-path graph distance between nodes i and j . After calculating the optimal scaling factor, c , we scale the embeddings by this factor and recalculate the distortions for all pathways in the dataset. We summarize the distortions in Figure 2(b). The mixed-curvature embeddings exhibit significantly lower mean distortion and variance than the node2vec and Laplacian baselines.

4.2. Edge Prediction

4.2.1. OVERVIEW

We train on individual pathway graphs to predict a set of held-out edges, then test our prediction models on the test set of experimentally validated edges from STRING. For each pathway, we determine its optimal embedding space using the results of our hyperparameter sweep for the distortion task. That is, for each pathway graph, we select the signature for the embedding space (number of hyperbolic, Euclidean, and spherical components, as well as their respective dimensionalities) that minimizes the distortion across the set of embeddings for that pathway graph. We then perform edge prediction on two different datasets:

In-Distribution An in-distribution validation set containing held-out edges from the original pathway graph. These edges are not seen by the model during training, but the

validation set performance metrics, such as validation accuracy and validation loss, are used to guide model training and hyperparameter selection. 95% of the edges from each pathway were used for training, and 5% were used for validation.

Out-of-Distribution An out-of-distribution test set that includes edges from the STRING PPI database. This dataset is not seen by the model during training and is *not* used to guide model training or hyperparameter selection. These edges are general PPIs and do not necessarily have the same biological context as the pathway. However, pathway edge predictions supported by a general PPI are more plausible than those that are not.

We expect that the Product GCN, initialized with the min-distortion product space embeddings, has a better inductive bias in its pretrained representations that more preferentially match the topology of each graph than any of the other baselines. Thus, we expect that the Product GCN should more accurately predict in-distribution edges held out from the original graph. Although we are less certain what the effect of introducing non-Euclidean geometry should be to the prediction of out-of-distribution edges from an external database, we would hope that the Product GCN would still outperform the other baselines on this task.

4.2.2. BASELINES AND PRODUCT GCN

We compare four different methods on the edge prediction task:

1. A Euclidean GCN initialized with pretrained node2vec embeddings.

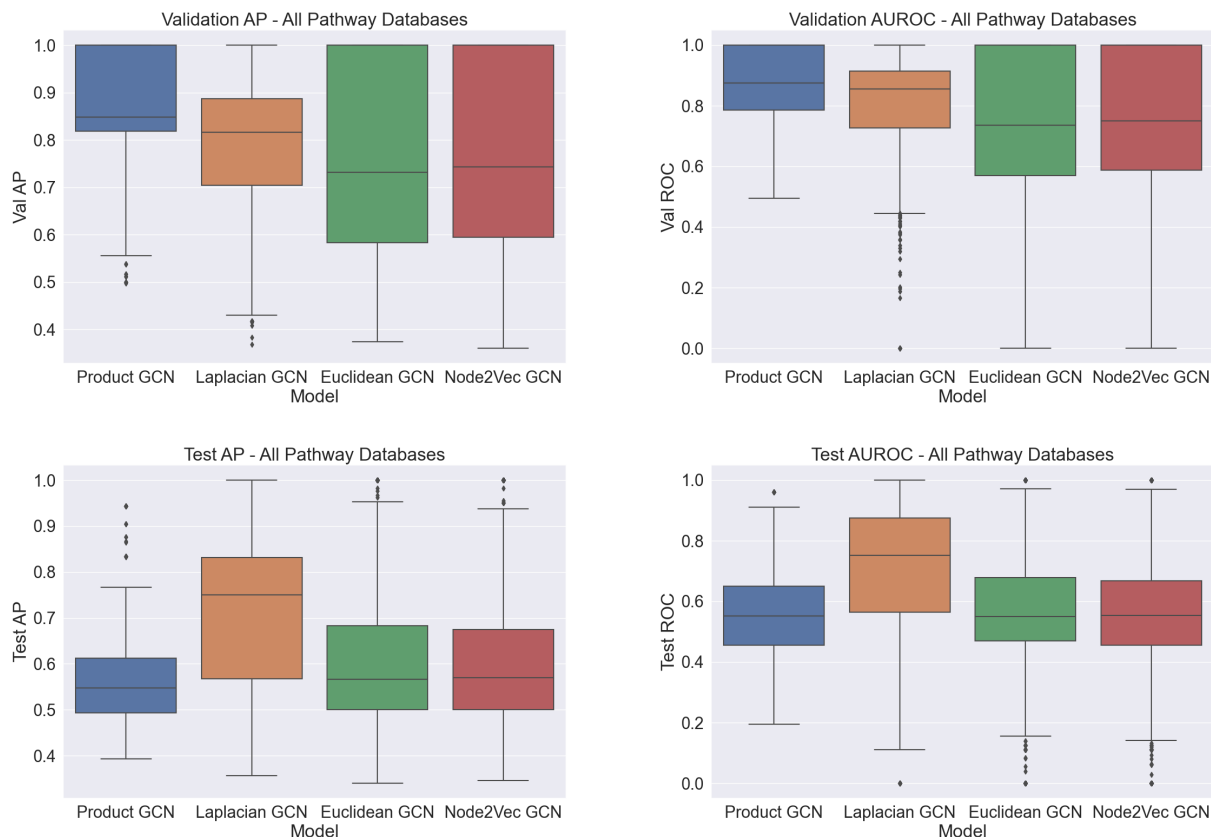


Figure 3. Edge prediction performance on all five pathway datasets for all models as given by four metrics: Validation Set AP, Validation Set AUROC, Test Set AP, and Test Set AUROC. Test set edges come from STRING.

2. A Euclidean GCN initialized with pretrained Laplacian embeddings.
3. A Euclidean GCN initialized with pretrained Euclidean embeddings designed to minimize distortion in \mathbb{R}^n .
4. A Product GCN architecture that matches the signature of the optimal non-Euclidean pathway embedding as measured by minimum distortion and is initialized with the pretrained mixed-curvature embeddings from the first task described in Section 4.1.

The pretrained Euclidean embeddings in method 3 are learned using the same Python package as is used for learning the mixed-curvature embeddings (Gu et al., 2019) but use a Euclidean manifold as the target output space. For all methods, we keep the total dimensionality of the embedding space fixed at 100 dimensions, with the exception of the Laplacian embedding method for which the embedding dimension was set to be the number of nodes in the graph, $|V|$. Since most pathway graphs have $|V| \leq 100$ (Figure 1(a)) the reduced dimensionality of the Laplacian embedding would be expected to be harmful, though it could provide

an outsized benefit in representational capacity for pathway graphs with a large number of nodes.

For the Product GCN, we match the signature of the best mixed-curvature embedding. For example, if the best embedding for pathway 21 of the PathBank dataset has the signature $\mathbb{H}^2 \times \mathbb{S}^3 \times \mathbb{E}^2$, then we use a Product GCN architecture with two hyperbolic manifold layers, three spherical manifold layers, and two Euclidean manifold layers. We furthermore split each node embedding into its constituent pieces as determined by the product manifold signature. In this example, the embedding would be split into $2+3+2 = 7$ slices, each of dimension 14. Each slice of the embedding is fed into the GCN for its corresponding manifold. Scores are then generated by each of the component GCNs and averaged to produce a final output score that is used to predict the presence of an edge between a given pair of nodes.

4.2.3. MODEL TRAINING

For each graph on which we perform edge prediction with the Product GCN, we perform a sweep over 324 hyperparameter combinations (Appendix) and choose the one with

the highest average of validation set AUROC and AP for use in downstream analyses. For the baseline methods, we perform a sweep over 108 hyperparameter configurations (Appendix). The difference in the two sweeps arises from the fact that the Product GCN has one additional hyperparameter, the curvature of the hyperbolic and spherical embedding spaces. We sweep over three values for this parameter, yielding three times as many hyperparameter configurations.

4.2.4. SUMMARY OF RESULTS

We find that mixed-curvature product manifold representations yield substantial benefits in representational capacity for boosting downstream edge performance on the in-distribution validation edges (Figure 3). The Product GCN initialized with pretrained product manifold representations outperforms, on average, all baselines for prediction of in-distribution validation set edges. Among the baseline methods, the graph Laplacian-based Euclidean GCN outperforms the two other Euclidean GCNs. For pathways with more than 100 nodes, this advantage is likely due to its larger embedding dimension. In the Appendix, we provide detailed paired comparisons of the AP and AUROC for the Product GCN and each Euclidean GCN on individual graphs in each pathway database.

The Product GCN does not have the same advantage over the baselines for the prediction of out-of-distribution PPI edges from STRING. The Euclidean GCN with pretrained graph Laplacian embeddings is the clear best model, and all others have near random AUROC. We surmise that the introduction of these edges induces a substantial distribution shift in the graph topologies, which makes the initially learned product space embeddings no longer a good fit. This causes the Product GCN to underperform relative to the Euclidean GCNs with their respective pretrained embeddings. One conclusion we can draw is that common Euclidean-style embeddings are more robust to distribution shifts of graph topology while product space embeddings, via their learned curvatures, impose a strong inductive bias to tree-like and ring-like structures in the graphs.

5. Discussion and Conclusion

We find that performing representation learning in non-Euclidean and mixed-curvature spaces yields notable improvements in distortion and downstream in-distribution edge prediction performance. In all cases, a mixed-curvature representation yields an embedding with lower distortion than a simple Euclidean embedding. However, the exact decomposition of the product space into its mixture of components is highly dependent on the graph topology. Thus, it is beneficial to perform a hyperparameter sweep over the number and types of components, as well as their dimen-

sionalities, when learning a representation for a biological pathway graph. Such a sweep need not be highly time intensive as biological pathway graphs are generally of a modest size.

For the out-of-distribution edge prediction task, the full structure of the graph is not known when the node embeddings are learned because the test set edges from STRING are not included in the training set. This leads to a number of questions about how to further generalize our approach. For example, we may ask how close the full graph structure must be to the observed structure in order to produce node embeddings that are usable for edge prediction via our method. We can also explore whether there are alternative hyperparameter tuning strategies that produce slightly worse distortions or in-distribution edge prediction performance but generalized better to out-of-distribution edge prediction. The Laplacian embedding has the best out-of-distribution performance, consistent with its robust behavior in previous biological graph representation learning benchmarking (Song et al., 2023). Currently, we only assess out-of-distribution edge predictions using STRING physical protein interactions. An evaluation of 45 interaction networks (Wright et al., 2025) could be used to prioritize other networks for evaluating these predictions and understand biases in the interaction networks.

Another future direction would be to consider additional downstream tasks, as edge prediction is not the only useful task for biological pathways that can be improved by non-Euclidean representation learning. We plan to investigate how our pathway embeddings benefit other problems such as node classification, for example, predicting the type (gene, protein, small molecule, metabolite, etc.) of a pathway node.

The lower performance of all models on the out-of-distribution edge prediction setting relative to the in-distribution setting may be partially attributable to biological context. Edges in a pathway reflect a pair of proteins that interact in the context of conducting some specific biological process, potentially only in certain cells or tissue types. The trained GCNs predict edges with that same context. However, the STRING-based evaluation lacks that context. There may be false negative edges in which there is a real PPI that is not relevant to the pathway. Alternatively, there may be false positive edges that are cell- or tissue-specific and not yet identified by the experiments aggregated into STRING.

Non-Euclidean embedding models have not been applied to pathway graphs, perhaps due to a lack of awareness among network biology researchers of their utility in reducing distortion of graph distances and improving downstream predictive performance. We demonstrate that pathway graphs benefit from the incorporation of non-Euclidean geometries

into embeddings and prediction models. We encourage researchers to consider making use of these non-standard geometries when learning embeddings and making downstream predictions.

Software and Data availability

We provide code at <https://github.com/mcneela/Mixed-Curvature-Pathways> and <https://github.com/mcneela/Mixed-Curvature-GCN>.

Acknowledgements

We thank David Merrell, Christopher Magnano, and Sam Gelman for their help in processing Pathway Commons graphs and generating visualizations. This research was supported by NIH award R01GM135631, the Wisconsin Alumni Research Foundation, and computing resources provided by the Center for High Throughput Computing (2006).

References

- Bachmann, G., Becigneul, G., and Ganea, O. Constant curvature graph convolutional networks. In III, H. D. and Singh, A. (eds.), *Proceedings of the 37th International Conference on Machine Learning*, volume 119 of *Proceedings of Machine Learning Research*, pp. 486–496. PMLR, 13–18 Jul 2020. URL <https://proceedings.mlr.press/v119/bachmann20a.html>.
- Becigneul, G. and Ganea, O.-E. Riemannian adaptive optimization methods. In *International Conference on Learning Representations*, 2019. URL <https://openreview.net/forum?id=rleiqi09K7>.
- Bonald, T. Spectral graph embedding - telecom paris, 2019. URL <https://perso.telecom-paristech.fr/bonald/documents/spectral.pdf>.
- Bonnabel, S. Stochastic gradient descent on Riemannian manifolds. *IEEE Transactions on Automatic Control*, 58(9):2217–2229, 2013. doi: 10.1109/TAC.2013.2254619.
- Bourgain, J. On Lipschitz embedding of finite metric spaces in Hilbert space. *Israel Journal of Mathematics*, 52(1): 46–52, 1985. doi: 10.1007/BF02776078.
- Center for High Throughput Computing. Center for high throughput computing. 2006. doi: 10.21231/GNT1-HW21.
- Chami, I., Ying, Z., Ré, C., and Leskovec, J. Hyperbolic graph convolutional neural networks. In *Advances in Neural Information Processing Systems*, pp. 4869–4880, 2019.
- Desai, K., Nickel, M., Rajpurohit, T., Johnson, J., and Vedantam, S. R. Hyperbolic image-text representations. In Krause, A., Brunskill, E., Cho, K., Engelhardt, B., Sabato, S., and Scarlett, J. (eds.), *Proceedings of the 40th International Conference on Machine Learning*, volume 202 of *Proceedings of Machine Learning Research*, pp. 7694–7731. PMLR, 23–29 Jul 2023. URL <https://proceedings.mlr.press/v202/desai23a.html>.
- Ding, J. and Regev, A. Deep generative model embedding of single-cell RNA-Seq profiles on hyperspheres and hyperbolic spaces. *Nature Communications*, 12(1):2554, May 2021. doi: 10.1038/s41467-021-22851-4.
- Durham, J., Zhang, J., Humphreys, I. R., Pei, J., and Cong, Q. Recent advances in predicting and modeling protein–protein interactions. *Trends in Biochemical Sciences*, 48(6):527–538, June 2023. doi: 10.1016/j.tibs.2023.03.003.
- Feng, J., Zeng, A., Chen, Y., Payne, P., and Li, F. Signaling interaction link prediction using deep graph neural networks integrating protein-protein interactions and omics data. *bioRxiv*, pp. 2020.12.23.424230, December 2020. doi: 10.1101/2020.12.23.424230.
- Ganea, O.-E., Bécigneul, G., and Hofmann, T. Hyperbolic Neural Networks. *arXiv:1805.09112*, June 2018. doi: 10.48550/arXiv.1805.09112.
- Gillespie, M., Jassal, B., Stephan, R., Milacic, M., Rothfels, K., Senff-Ribeiro, A., Griss, J., Sevilla, C., Matthews, L., Gong, C., Deng, C., Varusai, T., Ragueneau, E., Haider, Y., May, B., Shamovsky, V., Weiser, J., Brunson, T., Sannati, N., Beckman, L., Shao, X., Fabregat, A., Sidiropoulos, K., Murillo, J., Viteri, G., Cook, J., Shorsler, S., Bader, G., Demir, E., Sander, C., Haw, R., Wu, G., Stein, L., Hermjakob, H., and D’Eustachio, P. The Reactome pathway knowledgebase 2022. *Nucleic Acids Research*, 50(D1): D687–D692, January 2022. doi: 10.1093/nar/gkab1028.
- Giovanni, F. D., Luise, G., and Bronstein, M. M. Heterogeneous manifolds for curvature-aware graph embedding. In *ICLR 2022 Workshop on Geometrical and Topological Representation Learning*, 2022. URL <https://openreview.net/forum?id=rtUxsN-kaxc>.
- Grover, A. and Leskovec, J. node2vec: Scalable feature learning for networks. In *Proceedings of the 22nd ACM SIGKDD International Conference on Knowledge Discovery and Data Mining*, 2016.
- Gu, A., Sala, F., Gunel, B., and Ré, C. Learning mixed-curvature representations in product spaces. In *International Conference on Learning Representations*, 2019.

- Hagberg, A. A., Schult, D. A., and Swart, P. J. Exploring Network Structure, Dynamics, and Function using NetworkX. In *Proceedings of the 7th Python in Science Conference*, pp. 11–15, Pasadena, CA USA, 2008.
- Hanspers, K., Riutta, A., Summer-Kutmon, M., and Pico, A. R. Pathway information extracted from 25 years of pathway figures. *Genome Biology*, 21(1):273, November 2020. doi: 10.1186/s13059-020-02181-2.
- Hayakawa, J., Seki, T., Kawazoe, Y., and Ohe, K. Pathway importance by graph convolutional network and Shapley additive explanations in gene expression phenotype of diffuse large B-cell lymphoma. *PLOS ONE*, 17(6):e0269570, June 2022. doi: 10.1371/journal.pone.0269570.
- Jiang, J., Liu, L.-P., and Hassoun, S. Learning graph representations of biochemical networks and its application to enzymatic link prediction. *Bioinformatics*, 37(6):793–799, 10 2020. doi: 10.1093/bioinformatics/btaa881.
- Kanehisa, M., Goto, S., Sato, Y., Furumichi, M., and Tanabe, M. KEGG for integration and interpretation of large-scale molecular data sets. *Nucleic Acids Research*, 40(D1):D109–D114, January 2012. doi: 10.1093/nar/gkr988.
- Kim, J., Kim, D., and Sohn, K.-A. HiG2Vec: hierarchical representations of Gene Ontology and genes in the Poincaré ball. *Bioinformatics*, 37(18):2971–2980, September 2021. doi: 10.1093/bioinformatics/btab193.
- Klimovskaia, A., Lopez-Paz, D., Bottou, L., and Nickel, M. Poincaré maps for analyzing complex hierarchies in single-cell data. *Nature Communications*, 11(1):2966, June 2020. doi: 10.1038/s41467-020-16822-4.
- Lai, M., Chen, G., Yang, H., Yang, J., Jiang, Z., Wu, M., and Zheng, J. Predicting Synthetic Lethality in Human Cancers via Multi-Graph Ensemble Neural Network. In *43rd Annual International Conference of the IEEE Engineering in Medicine & Biology Society (EMBC)*, pp. 1731–1734, November 2021. doi: 10.1109/EMBC46164.2021.9630716.
- Lau, Y., Gutierrez, J. M., Volkovs, M., and Zuberi, S. Drug repurposing for Leishmaniasis with hyperbolic graph neural networks. *bioRxiv*, pp. 2023.02.11.528117, 2023. doi: 10.1101/2023.02.11.528117.
- Lee, J. M. *Introduction to Smooth Manifolds*, volume 218 of *Graduate Texts in Mathematics*. Springer, New York, NY, 2012. ISBN 978-1-4419-9981-8 978-1-4419-9982-5. doi: 10.1007/978-1-4419-9982-5. URL <https://link.springer.com/10.1007/978-1-4419-9982-5>.
- Lee, J. M. *Introduction to Riemannian Manifolds*, volume 176 of *Graduate Texts in Mathematics*. Springer International Publishing, Cham, 2018. ISBN 978-3-319-91754-2 978-3-319-91755-9. doi: 10.1007/978-3-319-91755-9. URL <http://link.springer.com/10.1007/978-3-319-91755-9>.
- Lee, S., Lim, S., Lee, T., Sung, I., and Kim, S. Cancer subtype classification and modeling by pathway attention and propagation. *Bioinformatics*, 36(12):3818–3824, June 2020. doi: 10.1093/bioinformatics/btaa203.
- Li, M. M., Huang, K., and Zitnik, M. Graph representation learning in biomedicine and healthcare. *Nature Biomedical Engineering*, 6(12):1353–1369, December 2022. doi: 10.1038/s41551-022-00942-x.
- Li, N., Yang, Z., Yang, Y., Wang, J., and Lin, H. Hyperbolic hierarchical knowledge graph embeddings for biological entities. *Journal of Biomedical Informatics*, 147:104503, November 2023. doi: 10.1016/j.jbi.2023.104503.
- Liang, B., Gong, H., Lu, L., and Xu, J. Risk stratification and pathway analysis based on graph neural network and interpretable algorithm. *BMC Bioinformatics*, 23(1):394, September 2022. doi: 10.1186/s12859-022-04950-1.
- Liu, L., Zhu, X., Ma, Y., Piao, H., Yang, Y., Hao, X., Fu, Y., Wang, L., and Peng, J. Combining sequence and network information to enhance protein–protein interaction prediction. *BMC Bioinformatics*, 21(16):537, 2020. doi: 10.1186/s12859-020-03896-6.
- M A Basher, A. R. and Hallam, S. J. Leveraging heterogeneous network embedding for metabolic pathway prediction. *Bioinformatics*, 37(6):822–829, 10 2020. doi: 10.1093/bioinformatics/btaa906.
- Macaulay, M., Darling, A., and Fourment, M. Fidelity of hyperbolic space for Bayesian phylogenetic inference. *PLOS Computational Biology*, 19(4):e1011084, April 2023. doi: 10.1371/journal.pcbi.1011084.
- Magnano, C. S. and Gitter, A. Graph algorithms for predicting subcellular localization at the pathway level. In *Pacific Symposium on Biocomputing*, pp. 145–156. World Scientific, 2023. ISBN 9789811270604. doi: 10.1142/9789811270611_0014. URL https://www.worldscientific.com/doi/10.1142/9789811270611_0014.
- McNeela, D., Sala, F., and Gitter, A. Mixed-curvature representation learning for biological pathway graphs. In *2023 ICML Workshop on Computational Biology*, Honolulu, Hawaii, USA, July 2023. URL https://icml-compbio.github.io/2023/papers/WCBICML2023_paper117.pdf.

- Mikolov, T., Sutskever, I., Chen, K., Corrado, G. S., and Dean, J. Distributed representations of words and phrases and their compositionality. In Burges, C., Bottou, L., Welling, M., Ghahramani, Z., and Weinberger, K. (eds.), *Advances in Neural Information Processing Systems*, volume 26. Curran Associates, Inc., 2013. URL https://proceedings.neurips.cc/paper_files/paper/2013/file/9aa42b31882ec039965f3c4923ce901b-Paper.pdf.
- Nickel, M. and Kiela, D. Poincaré embeddings for learning hierarchical representations. In Guyon, I., Luxburg, U. V., Bengio, S., Wallach, H., Fergus, R., Vishwanathan, S., and Garnett, R. (eds.), *Advances in Neural Information Processing Systems 30*, pp. 6338–6347. Curran Associates, Inc., 2017.
- Paszke, A., Gross, S., Massa, F., Lerer, A., Bradbury, J., Chanan, G., Killeen, T., Lin, Z., Gimelshein, N., Antiga, L., Desmaison, A., Kopf, A., Yang, E., DeVito, Z., Raison, M., Tejani, A., Chilamkurthy, S., Steiner, B., Fang, L., Bai, J., and Chintala, S. PyTorch: An Imperative Style, High-Performance Deep Learning Library. In *Advances in Neural Information Processing Systems*, volume 32, pp. 8024–8035. Curran Associates, Inc., 2019.
- Pershad, Y., Guo, M., and Altman, R. B. Pathway and network embedding methods for prioritizing psychiatric drugs. *Pacific Symposium on Biocomputing*, 25:671–682, 2020.
- Pham, C. and Dang, T. Link Prediction for Biomedical Network. In *The 12th International Conference on Advances in Information Technology*, IAIT2021, pp. 1–5, New York, NY, USA, July 2021. Association for Computing Machinery. ISBN 978-1-4503-9012-5. doi: 10.1145/3468784.3471608. URL <https://dl.acm.org/doi/10.1145/3468784.3471608>.
- Pogány, D. and Antal, P. Hyperbolic Manifold Learning on Differential Expression Signatures. *TechRxiv*, December 2023. doi: 10.36227/techrxiv.24630747.v1.
- Pogány, D. and Antal, P. Towards explainable interaction prediction: Embedding biological hierarchies into hyperbolic interaction space. *PLoS ONE*, 19(3):e0300906, March 2024. doi: 10.1371/journal.pone.0300906.
- Poleksic, A. Hyperbolic matrix factorization improves prediction of drug-target associations. *Scientific Reports*, 13(1):959, January 2023. doi: 10.1038/s41598-023-27995-5.
- Rodchenkov, I., Babur, O., Luna, A., Aksoy, B. A., Wong, J. V., Fong, D., Franz, M., Siper, M. C., Cheung, M., Wrana, M., Mistry, H., Mosier, L., Dlin, J., Wen, Q., O’Callaghan, C., Li, W., Elder, G., Smith, P. T., Dallago, C., Cerami, E., Gross, B., Dogrusoz, U., Demir, E., Bader, G. D., and Sander, C. Pathway Commons 2019 Update: integration, analysis and exploration of pathway data. *Nucleic Acids Research*, 48(D1):D489–D497, January 2020. doi: 10.1093/nar/gkz946.
- Romero, P., Wagg, J., Green, M. L., Kaiser, D., Krummenacker, M., and Karp, P. D. Computational prediction of human metabolic pathways from the complete human genome. *Genome Biology*, 6(1):R2, December 2004. doi: 10.1186/gb-2004-6-1-r2.
- Sala, F., De Sa, C., Gu, A., and Re, C. Representation trade-offs for hyperbolic embeddings. In Dy, J. and Krause, A. (eds.), *Proceedings of the 35th International Conference on Machine Learning*, volume 80 of *Proceedings of Machine Learning Research*, pp. 4460–4469. PMLR, July 2018. URL <https://proceedings.mlr.press/v80/sala18a.html>.
- Schaefer, C. F., Anthony, K., Krupa, S., Buchoff, J., Day, M., Hannay, T., and Buetow, K. H. PID: the Pathway Interaction Database. *Nucleic Acids Research*, 37(suppl 1):D674–D679, January 2009. doi: 10.1093/nar/gkn653.
- Song, Z., Baur, B., and Roy, S. Benchmarking graph representation learning algorithms for detecting modules in molecular networks. *F1000Research*, August 2023. doi: 10.12688/f1000research.134526.1.
- Susmelj, A. K., Ren, Y., Vander Meersche, Y., Gelly, J.-C., and Galochkina, T. Poincaré maps for visualization of large protein families. *Briefings in Bioinformatics*, 24(3):bbad103, May 2023. doi: 10.1093/bib/bbad103.
- Szklarczyk, D., Kirsch, R., Koutrouli, M., Nastou, K., Mehryary, F., Hachilif, R., Gable, A. L., Fang, T., Doncheva, N. T., Pyysalo, S., Bork, P., Jensen, L. J., and von Mering, C. The STRING database in 2023: protein–protein association networks and functional enrichment analyses for any sequenced genome of interest. *Nucleic Acids Research*, 51(D1):D638–D646, January 2023. doi: 10.1093/nar/gkac1000.
- Tseng, A., Yu, T., Liu, T. J., and Sa, C. D. Coneheads: Hierarchy aware attention. In *Thirty-seventh Conference on Neural Information Processing Systems*, 2023. URL <https://openreview.net/forum?id=CzAFnfwbGd>.
- Tu, L. W. *An Introduction to Manifolds*. Universitext. Springer, New York, NY, 1 edition, 2008. ISBN 978-0-387-48098-5 978-0-387-48101-2. doi: 10.1007/978-0-387-48101-2. URL <http://link.springer.com/10.1007/978-0-387-48101-2>.

- Wishart, D. S., Li, C., Marcu, A., Badran, H., Pon, A., Budinski, Z., Patron, J., Lipton, D., Cao, X., Oler, E., Li, K., Paccoud, M., Hong, C., Guo, A. C., Chan, C., Wei, W., and Ramirez-Gaona, M. PathBank: a comprehensive pathway database for model organisms. *Nucleic Acids Research*, 48(D1):D470–D478, January 2020. doi: 10.1093/nar/gkz861.
- Wright, S. N., Colton, S., Schaffer, L. V., Pillich, R. T., Churas, C., Pratt, D., and Ideker, T. State of the interactomes: an evaluation of molecular networks for generating biological insights. *Molecular Systems Biology*, 21(1): 1–29, January 2025. doi: 10.1038/s44320-024-00077-y.
- Wu, Z., Pan, S., Chen, F., Long, G., Zhang, C., and Yu, P. S. A Comprehensive Survey on Graph Neural Networks. *IEEE Transactions on Neural Networks and Learning Systems*, 32(1):4–24, January 2021. doi: 10.1109/TNNLS.2020.2978386.
- Xin, J., Mark, A., Afrasiabi, C., Tsueng, G., Juchler, M., Gopal, N., Stupp, G. S., Putman, T. E., Ainscough, B. J., Griffith, O. L., Torkamani, A., Whetzel, P. L., Mungall, C. J., Mooney, S. D., Su, A. I., and Wu, C. High-performance web services for querying gene and variant annotation. *Genome Biology*, 17(1):91, 2016. doi: 10.1186/s13059-016-0953-9.
- Yang, J., Liu, Z., Zhang, M., and Wang, S. Pathway2Text: Dataset and Method for Biomedical Pathway Description Generation. In *Findings of the Association for Computational Linguistics: NAACL 2022*, pp. 1441–1454, Seattle, United States, July 2022. Association for Computational Linguistics. doi: 10.18653/v1/2022.findings-naacl.108. URL <https://aclanthology.org/2022.findings-naacl.108>.
- Yue, Y., McDonald, D., Hao, L., Lei, H., Butler, M. S., and He, S. FLONE: fully Lorentz network embedding for inferring novel drug targets. *Bioinformatics Advances*, 3(1):vbad066, May 2023. doi: 10.1093/bioadv/vbad066.
- Zahra, N. u. A., Vagiona, A.-C., Uddin, R., and Andrade-Navarro, M. A. Selection of Multi-Drug Targets against Drug-Resistant Mycobacterium tuberculosis XDR1219 Using the Hyperbolic Mapping of the Protein Interaction Network. *International Journal of Molecular Sciences*, 24(18):14050, January 2023. doi: 10.3390/ijms241814050.
- Zhang, D. and Kabuka, M. Multimodal deep representation learning for protein interaction identification and protein family classification. *BMC Bioinformatics*, 20(16):531, 2019. doi: 10.1186/s12859-019-3084-y.
- Zhou, Y. and Sharpee, T. O. Hyperbolic geometry of gene expression. *iScience*, 24(3), March 2021. doi: 10.1016/j.isci.2021.102225.

Appendix

A. Supplementary Methods

A.1. Pathway Commons Data

We use the Pathway Commons v12 PathBank pathways provided in this file: <https://www.pathwaycommons.org/archives/PC2/v12/PathwayCommons12.pathbank.hgnc.txt.gz>

Pathway Commons provides a number of different data formats, including text, SIF, JSON, and BioPAX. We use the text format as it provides the simplest graph representation of the most important interactions in PathBank pathways.

A.2. Initializing GCNs with Embeddings

We save the embeddings learned by the embedding model in a PyTorch .pt file (Paszke et al., 2019). We then load these embeddings and use them to initialize the weights of the embedding layer for the models in the edge prediction task, namely the Euclidean GCN and Product GCN. These embeddings are then further trained via backpropagation during the edge prediction task.

B. Supplementary Tables

learning rate	hyperbolic components	Euclidean components	spherical components
1e-3	0	0	0
1e-2	1	1	1
1e-1	2	2	2
1	3	3	3

Table 2: Range of values for the pathway embedding hyperparameter sweep. Space dimensions were calculated automatically (to sum to 100) based on the number of components of each space. For example, if there were 2 hyperbolic components, 1 Euclidean component, and 3 spherical components, then there would be $\text{floor}(100/6) = 16$ dimensions assigned to each component.

learning rate	hidden dim	# of layers	dropout	use bias	curvature (for Product GCN)
1e-4	16	2	0.1	true	0.5
1e-3	32	3	0.2	false	1
1e-2	64	4			2

Table 3: Hyperparameters used in the sweep for training the edge prediction GCNs.

C. Supplementary Figures

Product Manifold Representations for Learning on Biological Pathways

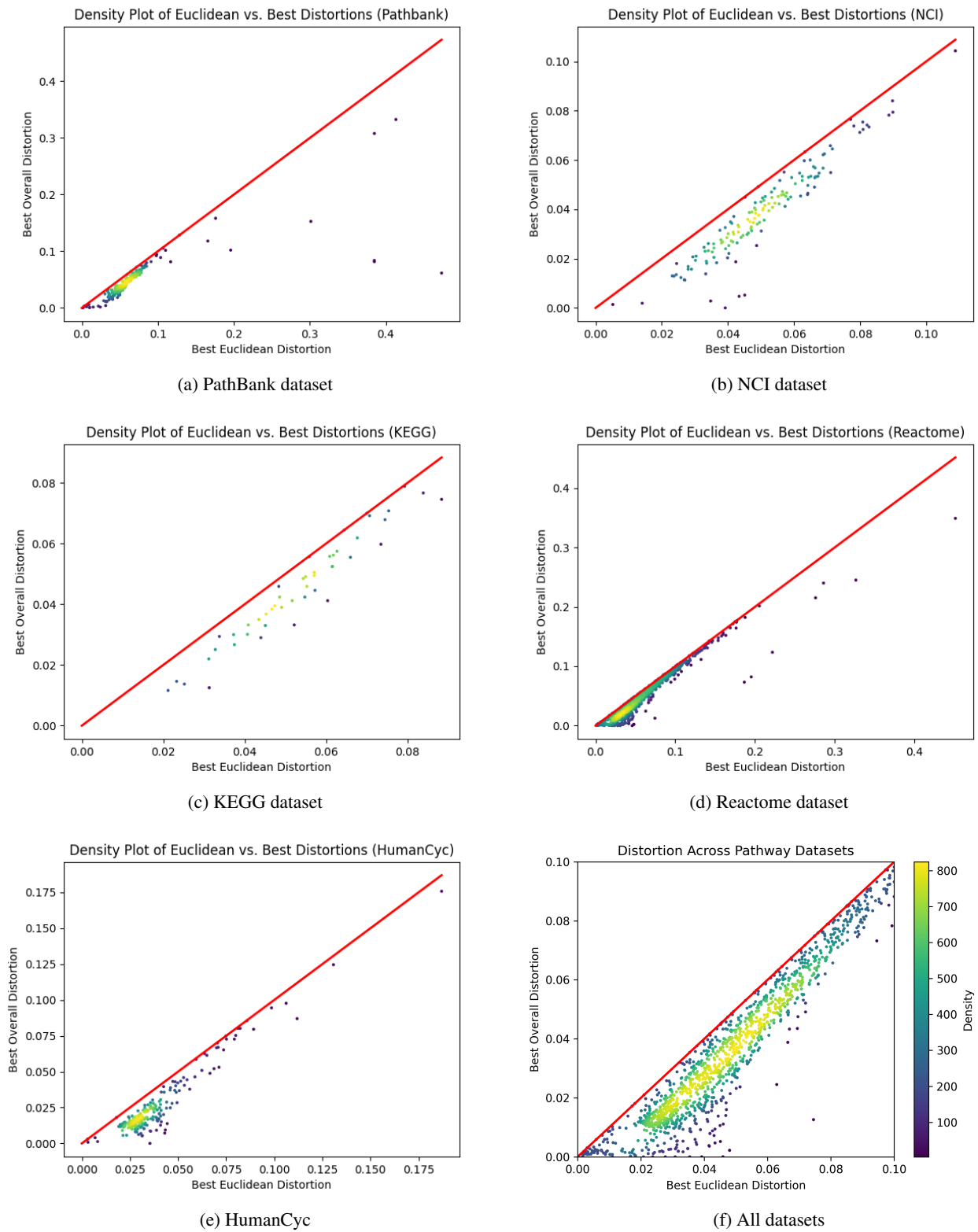


Figure 4. Scatterplots of distortion in the Euclidean embedding versus distortion in the mixed-curvature embedding for pathway datasets. Points are colored by local density, with yellow indicating the highest density.

C.1. PathBank

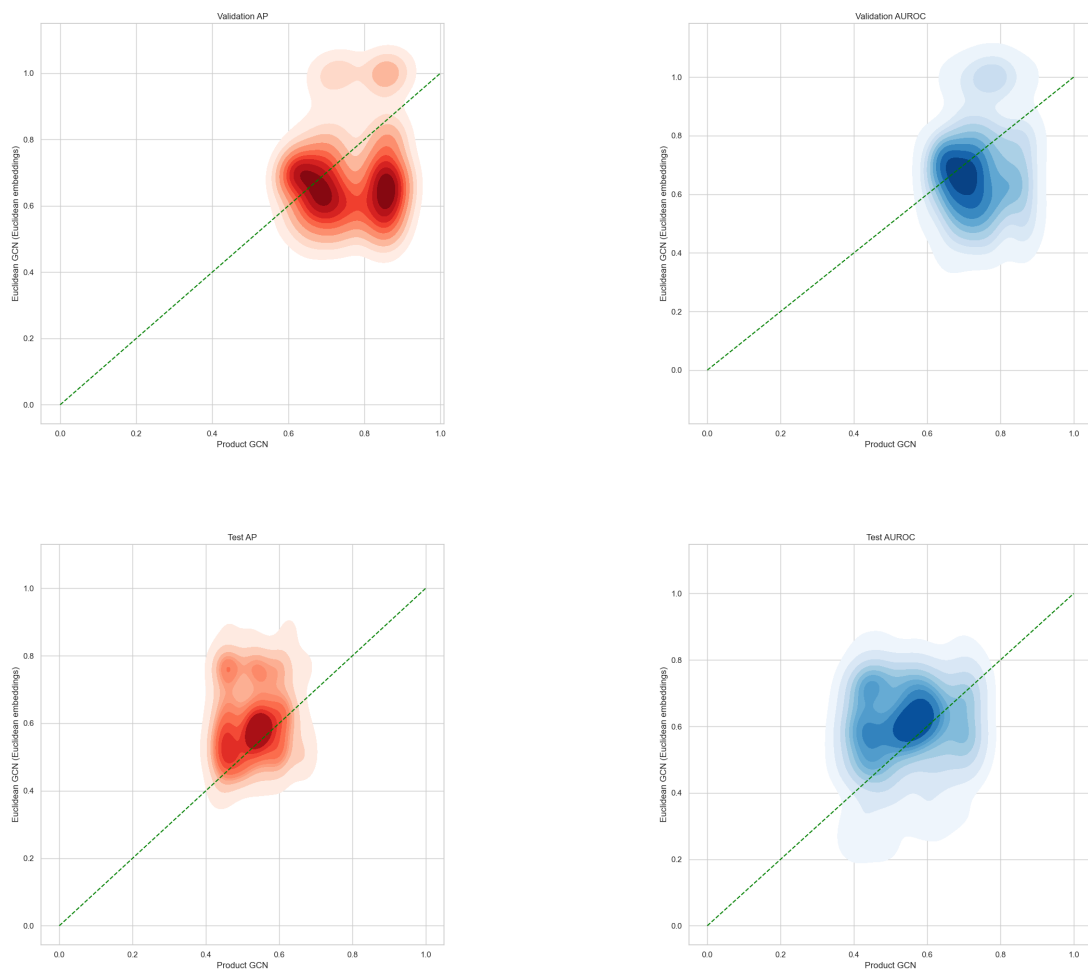


Figure 5. Comparison of Euclidean GCN initialized with pretrained Euclidean embeddings and Product GCN performance on in-distribution validation set and out-of-distribution test set. Each density plot shows one of either AP or AUROC metrics taken across all graphs in the PathBank dataset.

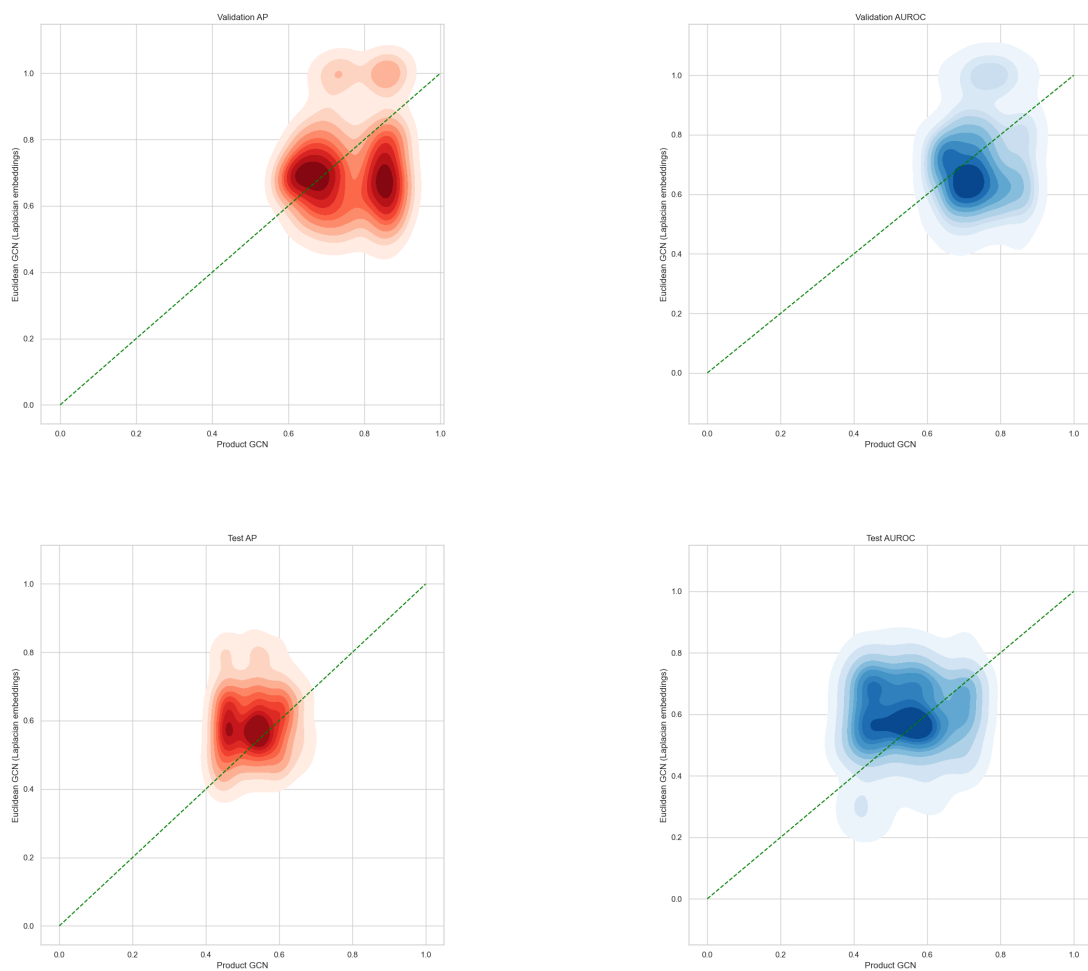


Figure 6. Comparison of Euclidean GCN initialized with pretrained Laplacian embeddings and Product GCN performance on in-distribution validation set and out-of-distribution test set. Each density plot shows one of either AP or AUROC metrics taken across all graphs in the PathBank dataset.

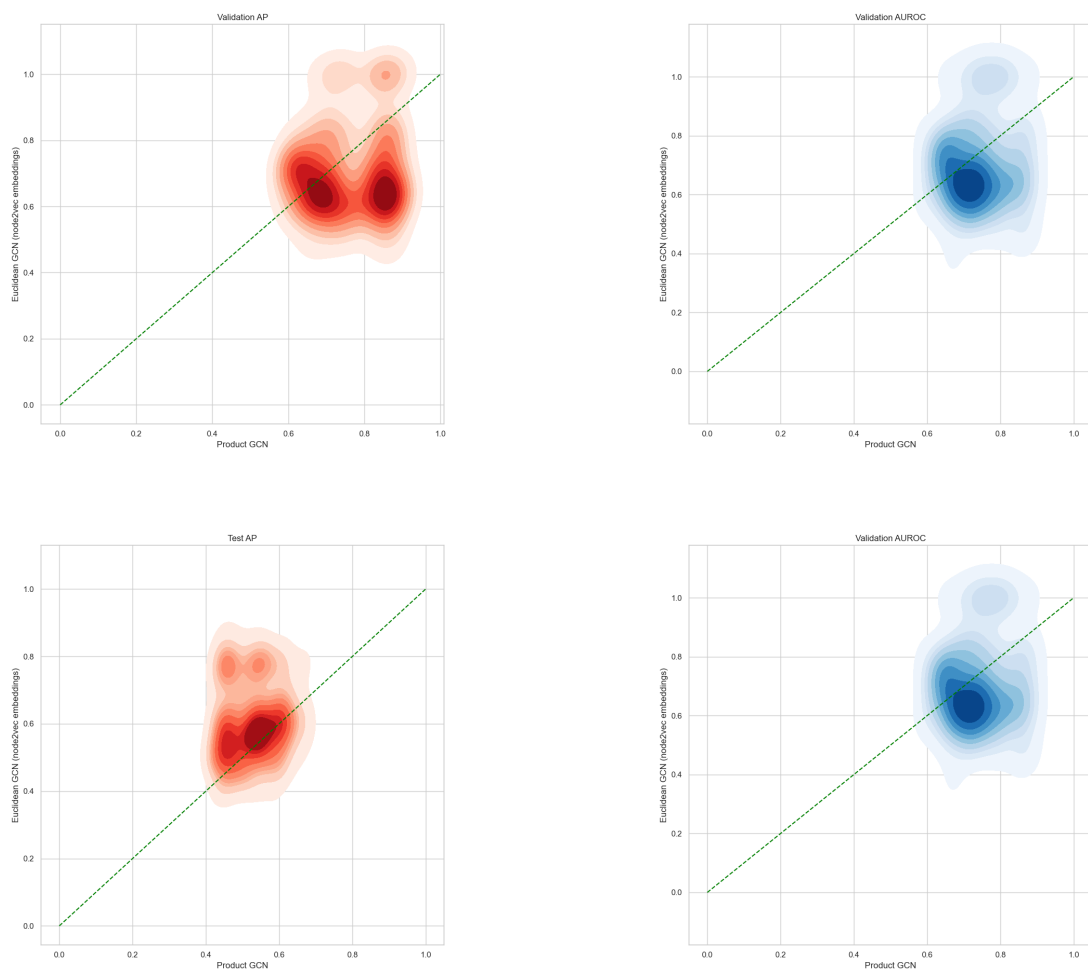


Figure 7. Comparison of Euclidean GCN initialized with pretrained node2vec embeddings and Product GCN performance on in-distribution validation set and out-of-distribution test set. Each density plot shows one of either AP or AUROC metrics taken across all graphs in the PathBank dataset.

C.2. Reactome

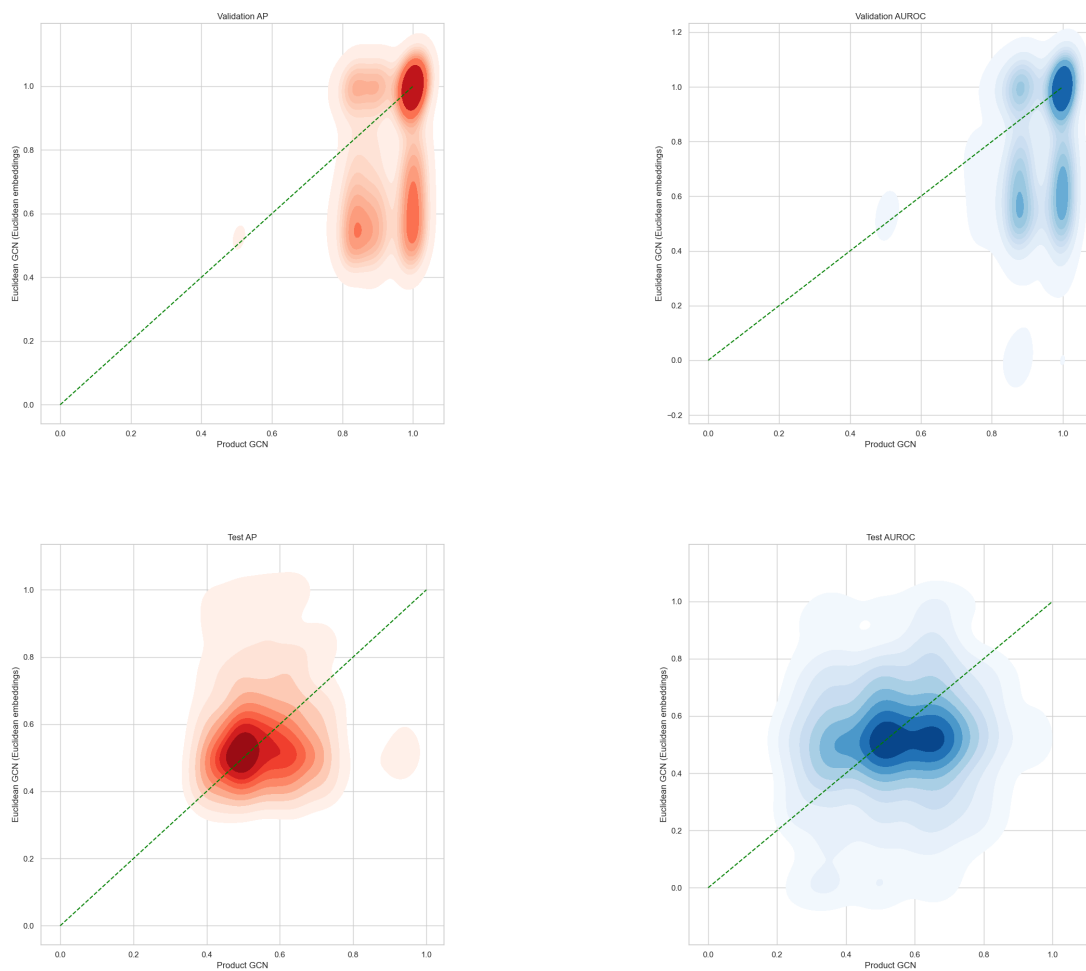


Figure 8. Comparison of Euclidean GCN initialized with pretrained Euclidean embeddings and Product GCN performance on in-distribution validation set and out-of-distribution test set. Each density plot shows one of either AP or AUROC metrics taken across all graphs in the Reactome dataset.

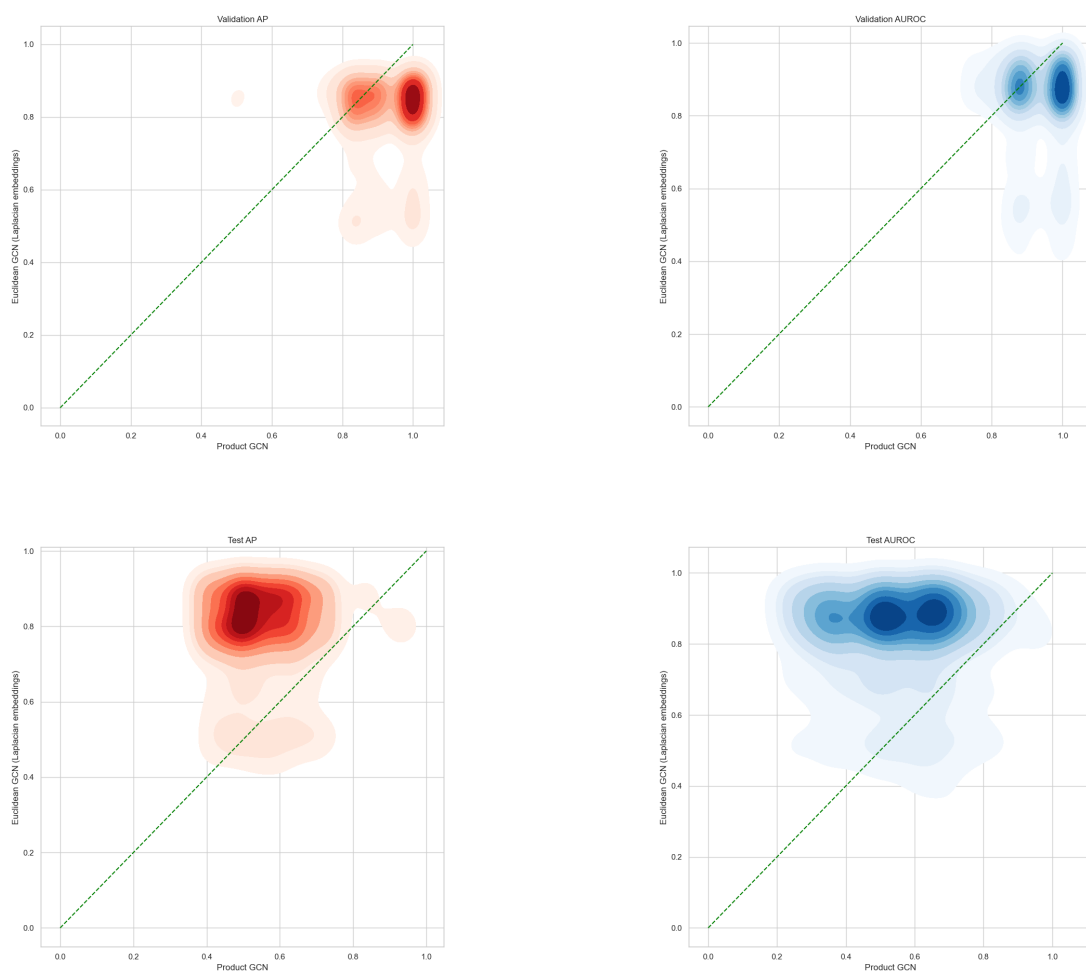


Figure 9. Comparison of Euclidean GCN initialized with pretrained Laplacian embeddings and Product GCN performance on in-distribution validation set and out-of-distribution test set. Each density plot shows one of either AP or AUROC metrics taken across all graphs in the Reactome dataset.

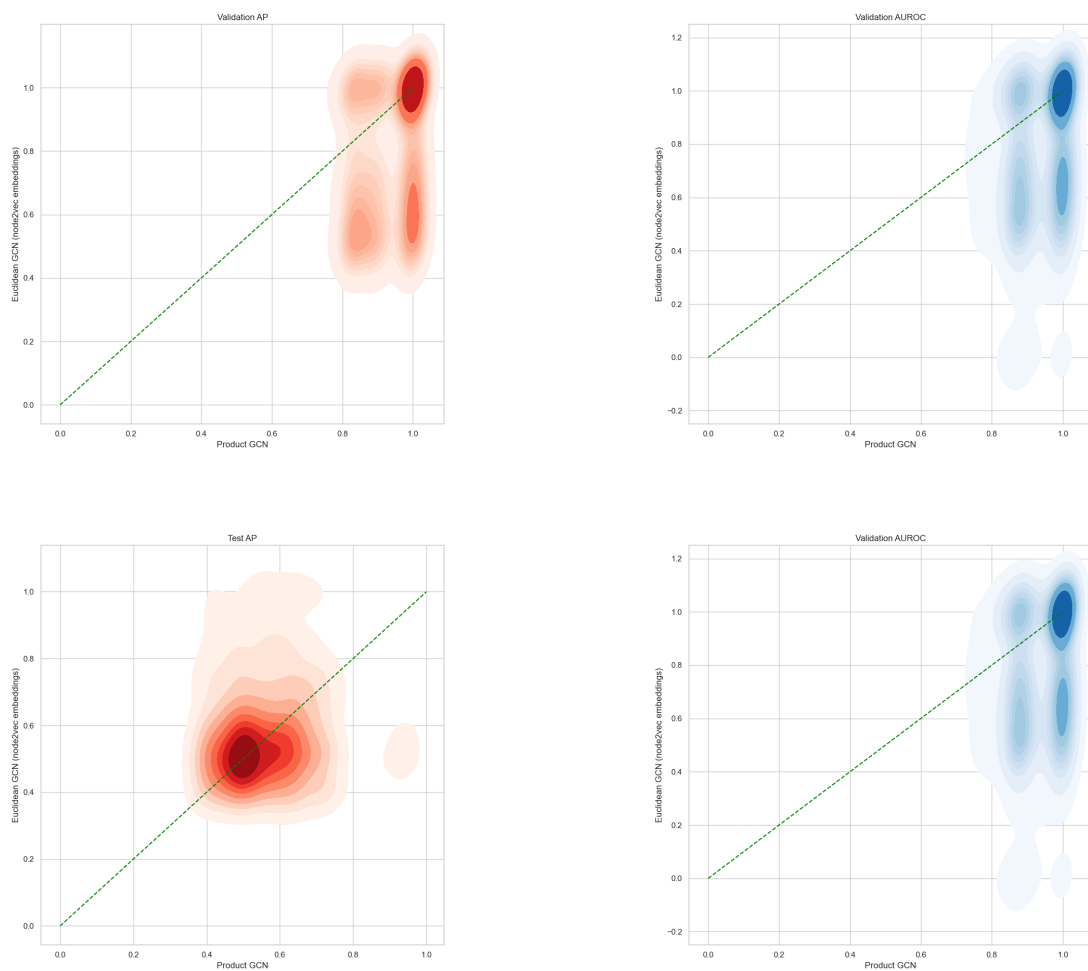


Figure 10. Comparison of Euclidean GCN initialized with pretrained node2vec embeddings and Product GCN performance on in-distribution validation set and out-of-distribution test set. Each density plot shows one of either AP or AUROC metrics taken across all graphs in the Reactome dataset.

C.3. HumanCyc

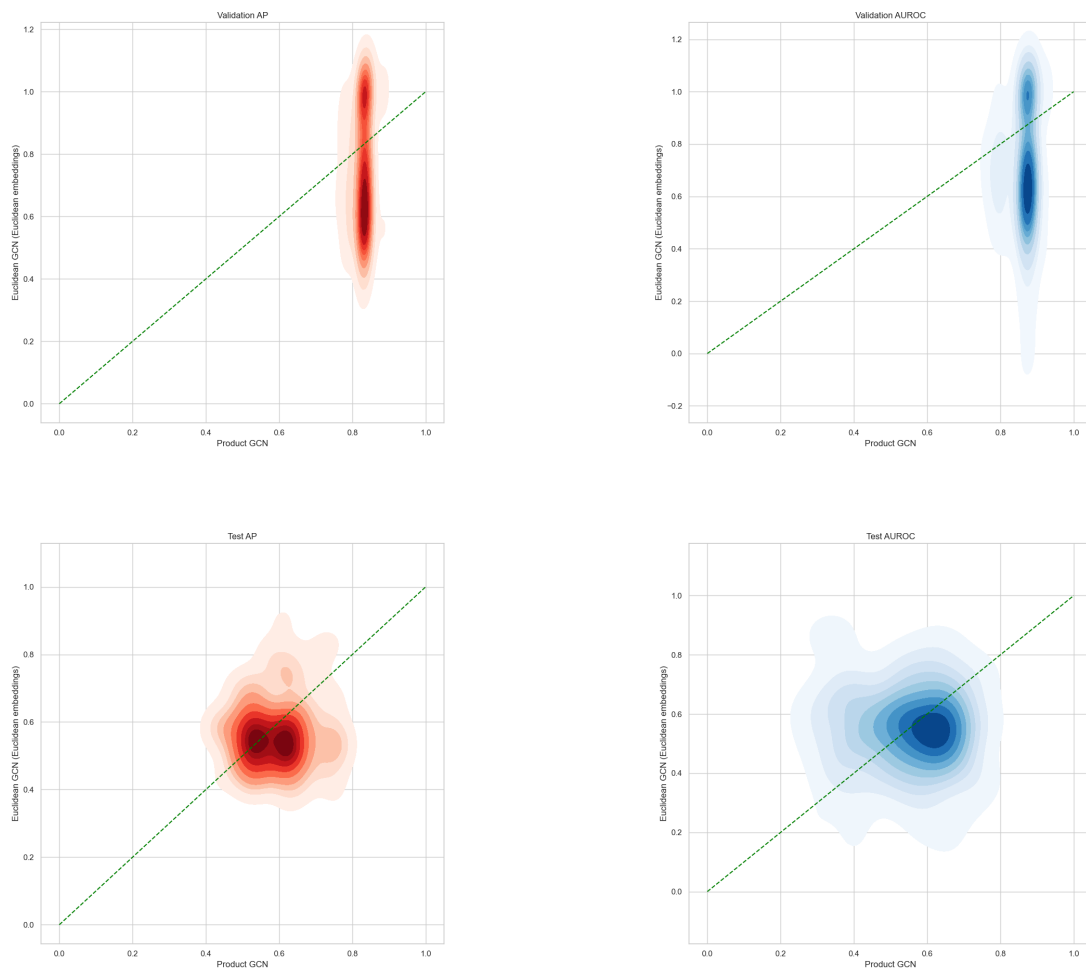


Figure 11. Comparison of Euclidean GCN initialized with pretrained Euclidean embeddings and Product GCN performance on in-distribution validation set and out-of-distribution test set. Each density plot shows one of either AP or AUROC metrics taken across all graphs in the HumanCyc dataset.

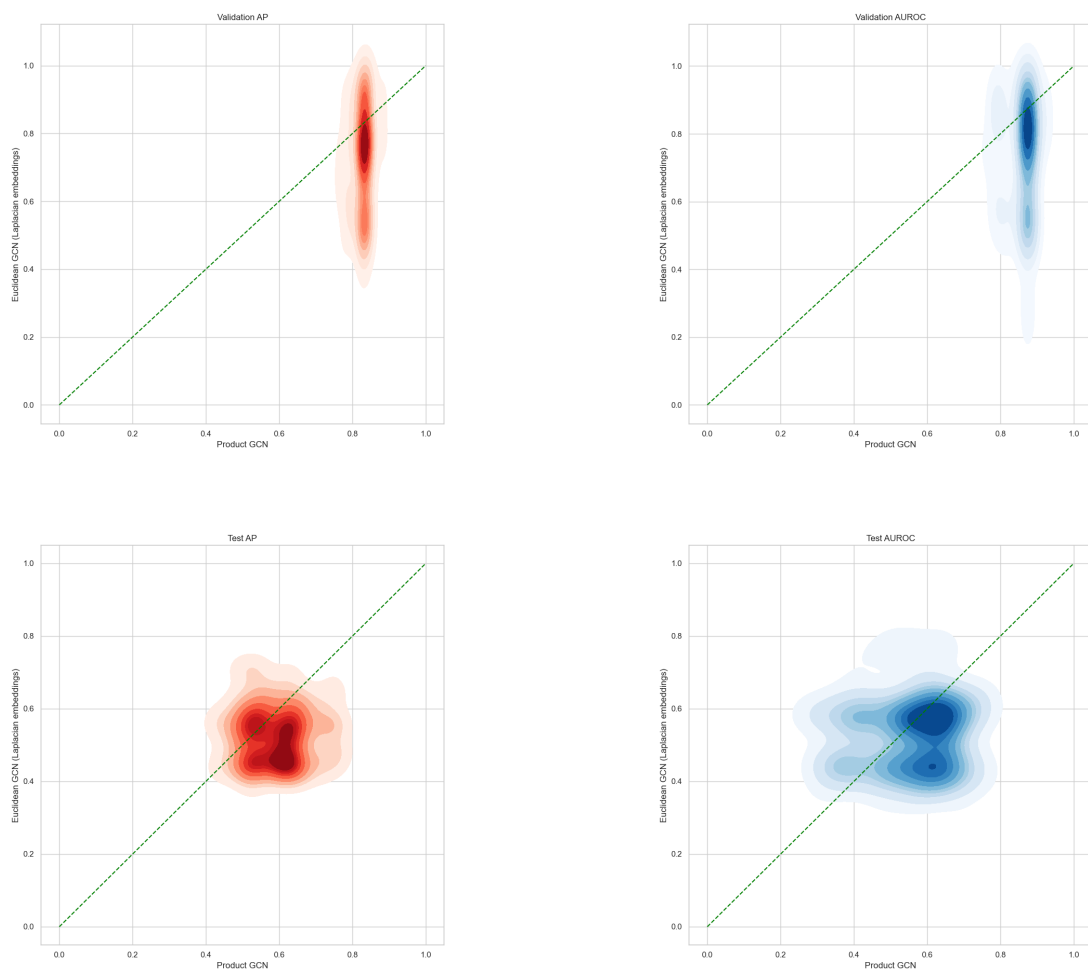


Figure 12. Comparison of Euclidean GCN initialized with pretrained Laplacian embeddings and Product GCN performance on in-distribution validation set and out-of-distribution test set. Each density plot shows one of either AP or AUROC metrics taken across all graphs in the HumanCyc dataset.

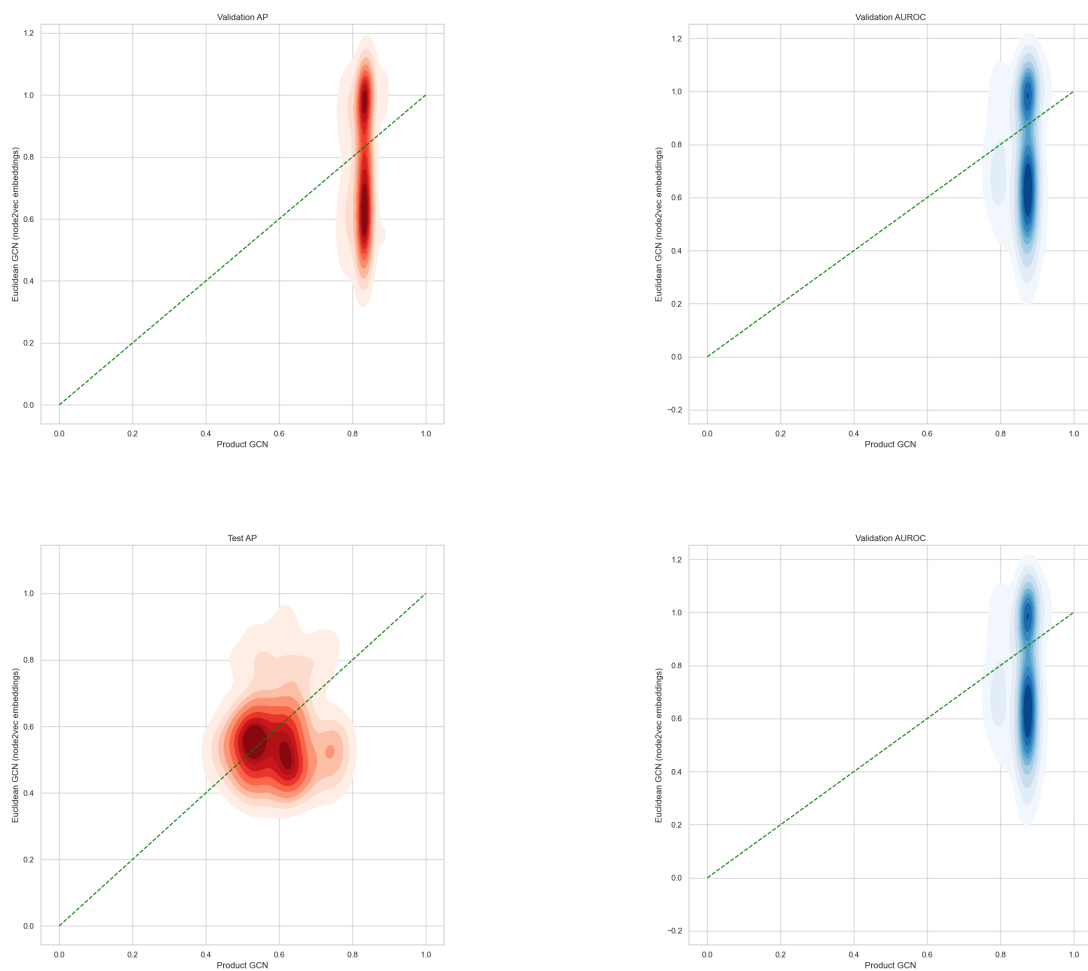


Figure 13. Comparison of Euclidean GCN initialized with pretrained node2vec embeddings and Product GCN performance on in-distribution validation set and out-of-distribution test set. Each density plot shows one of either AP or AUROC metrics taken across all graphs in the HumanCyc dataset.

C.4. NCI

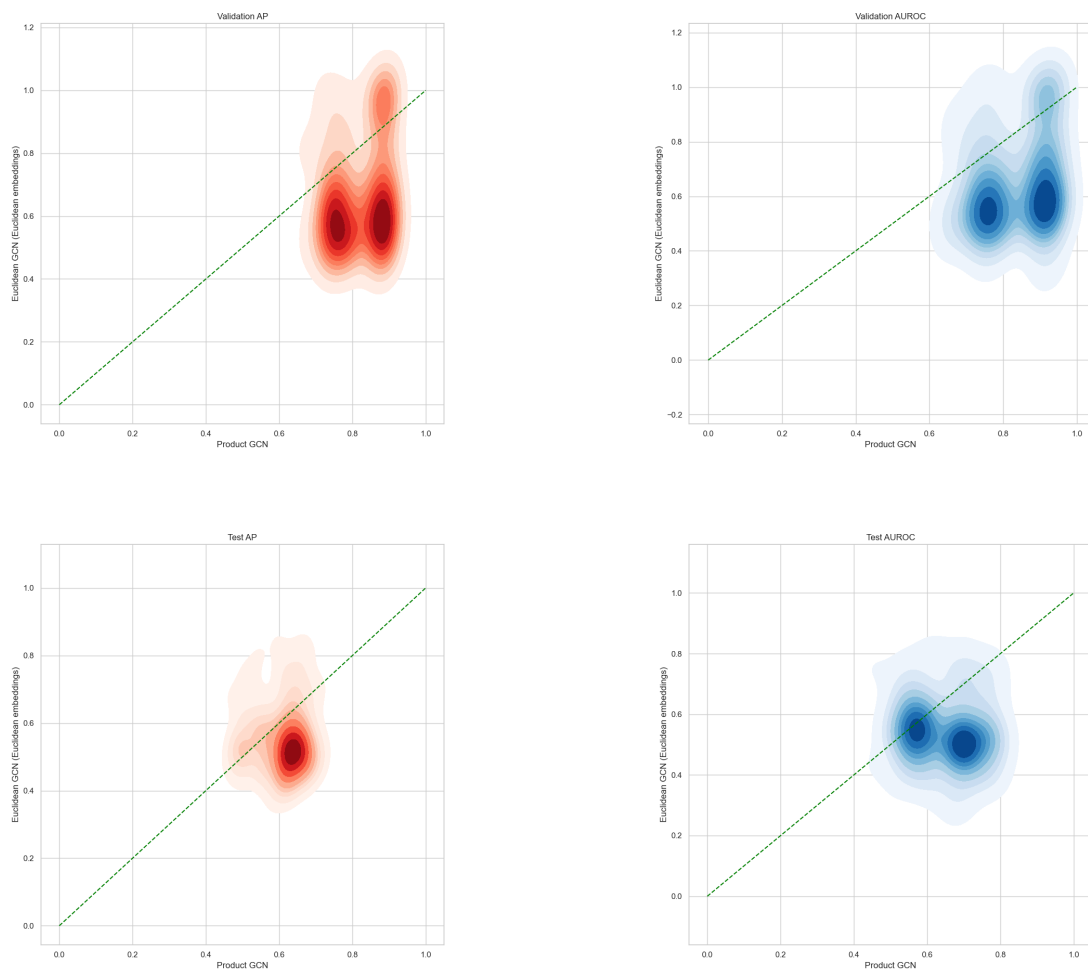


Figure 14. Comparison of Euclidean GCN initialized with pretrained Euclidean embeddings and Product GCN performance on in-distribution validation set and out-of-distribution test set. Each density plot shows one of either AP or AUROC metrics taken across all graphs in the NCI dataset.

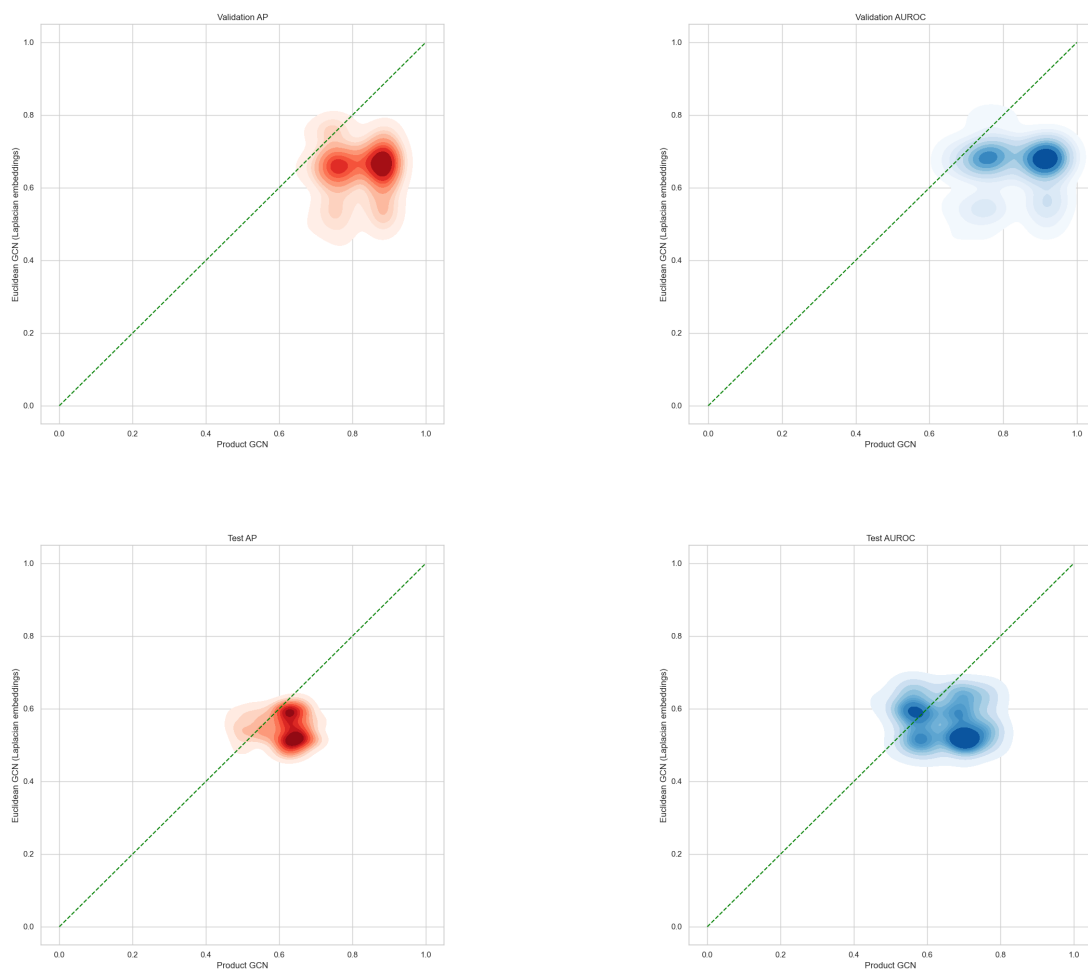


Figure 15. Comparison of Euclidean GCN initialized with pretrained Laplacian embeddings and Product GCN performance on in-distribution validation set and out-of-distribution test set. Each density plot shows one of either AP or AUROC metrics taken across all graphs in the NCI dataset.

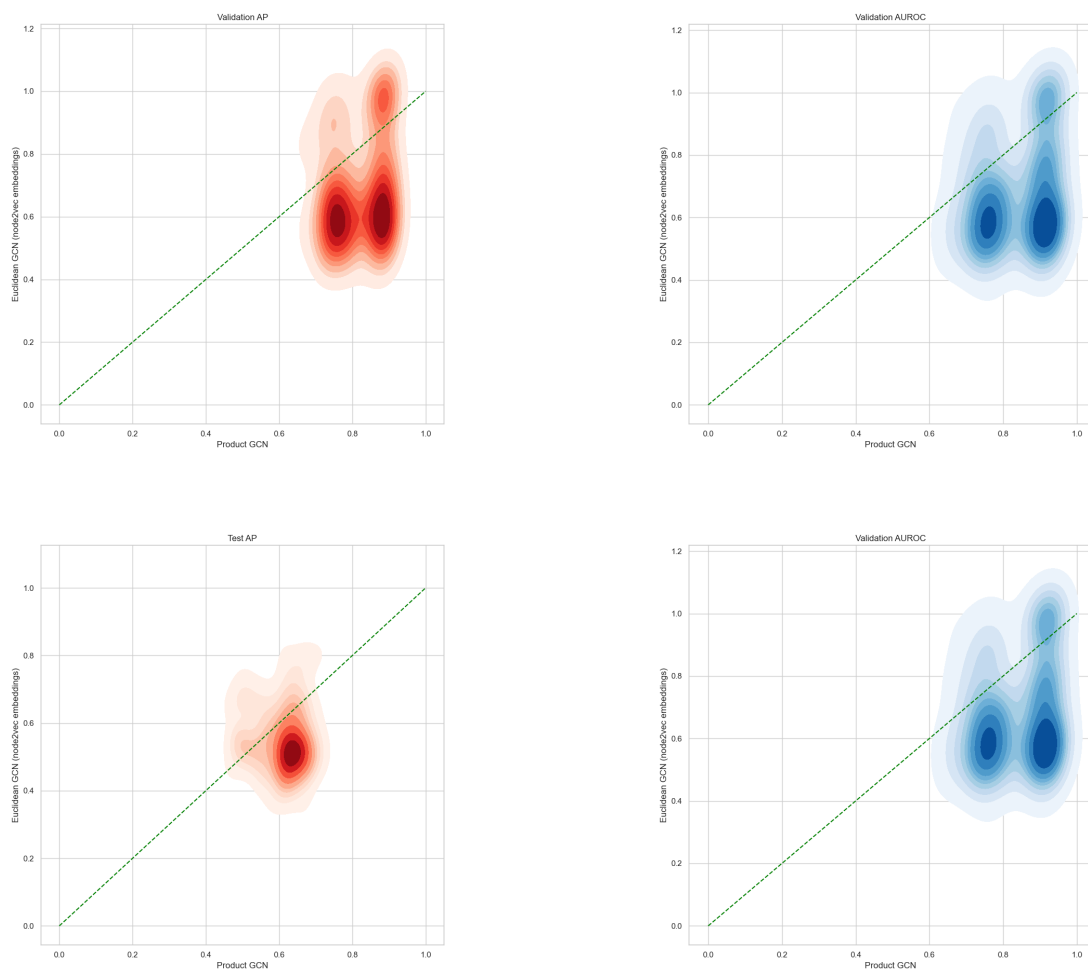


Figure 16. Comparison of Euclidean GCN initialized with pretrained node2vec embeddings and Product GCN performance on in-distribution validation set and out-of-distribution test set. Each density plot shows one of either AP or AUROC metrics taken across all graphs in the NCI dataset.

C.5. KEGG

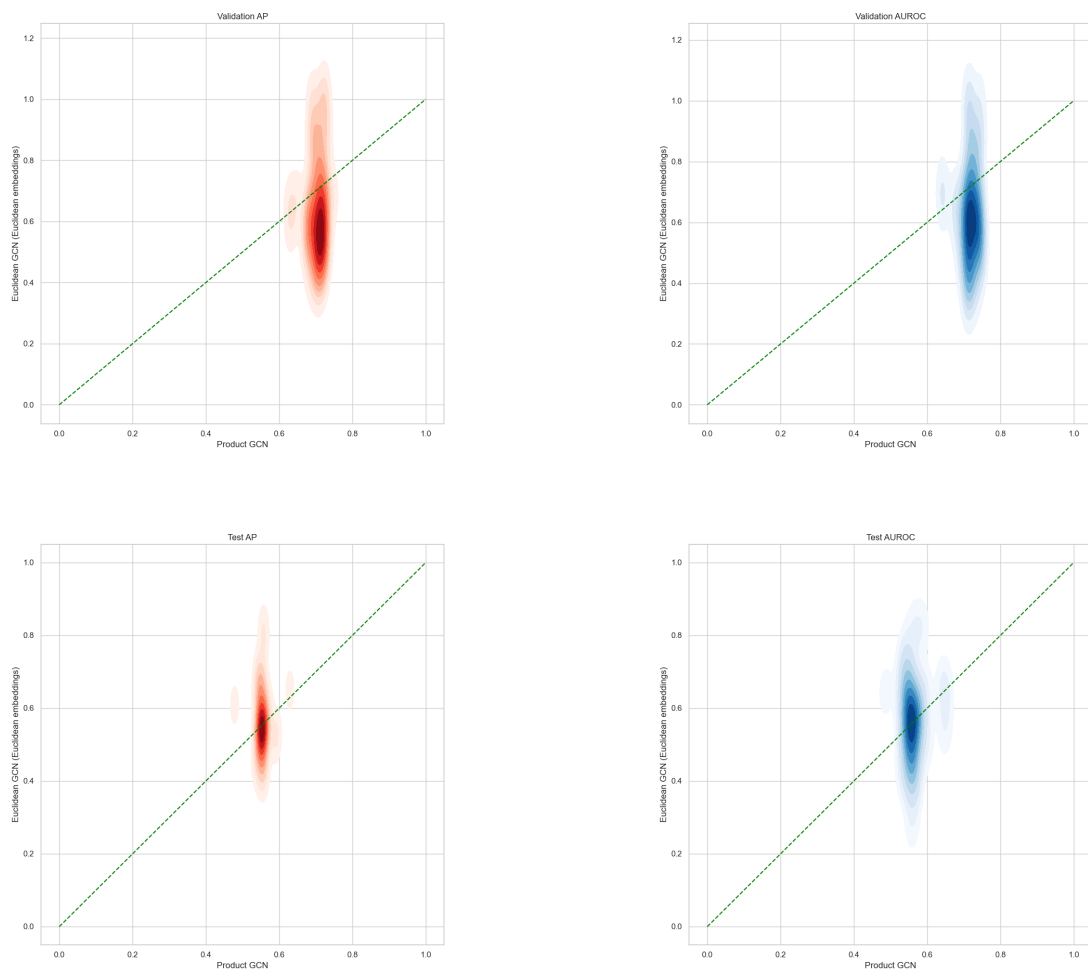


Figure 17. Comparison of Euclidean GCN initialized with pretrained Euclidean embeddings and Product GCN performance on in-distribution validation set and out-of-distribution test set. Each density plot shows one of either AP or AUROC metrics taken across all graphs in the KEGG dataset.

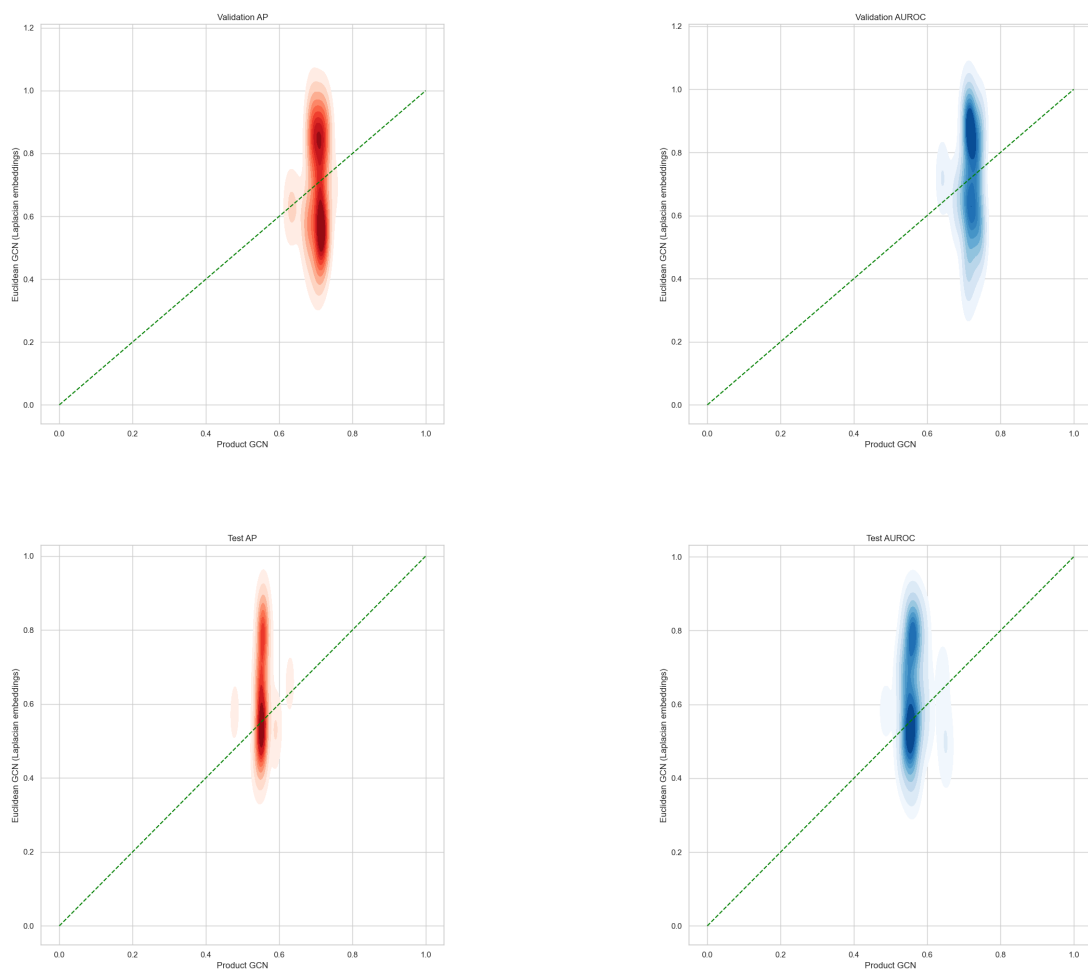


Figure 18. Comparison of Euclidean GCN initialized with pretrained Laplacian embeddings and Product GCN performance on in-distribution validation set and out-of-distribution test set. Each density plot shows one of either AP or AUROC metrics taken across all graphs in the KEGG dataset.

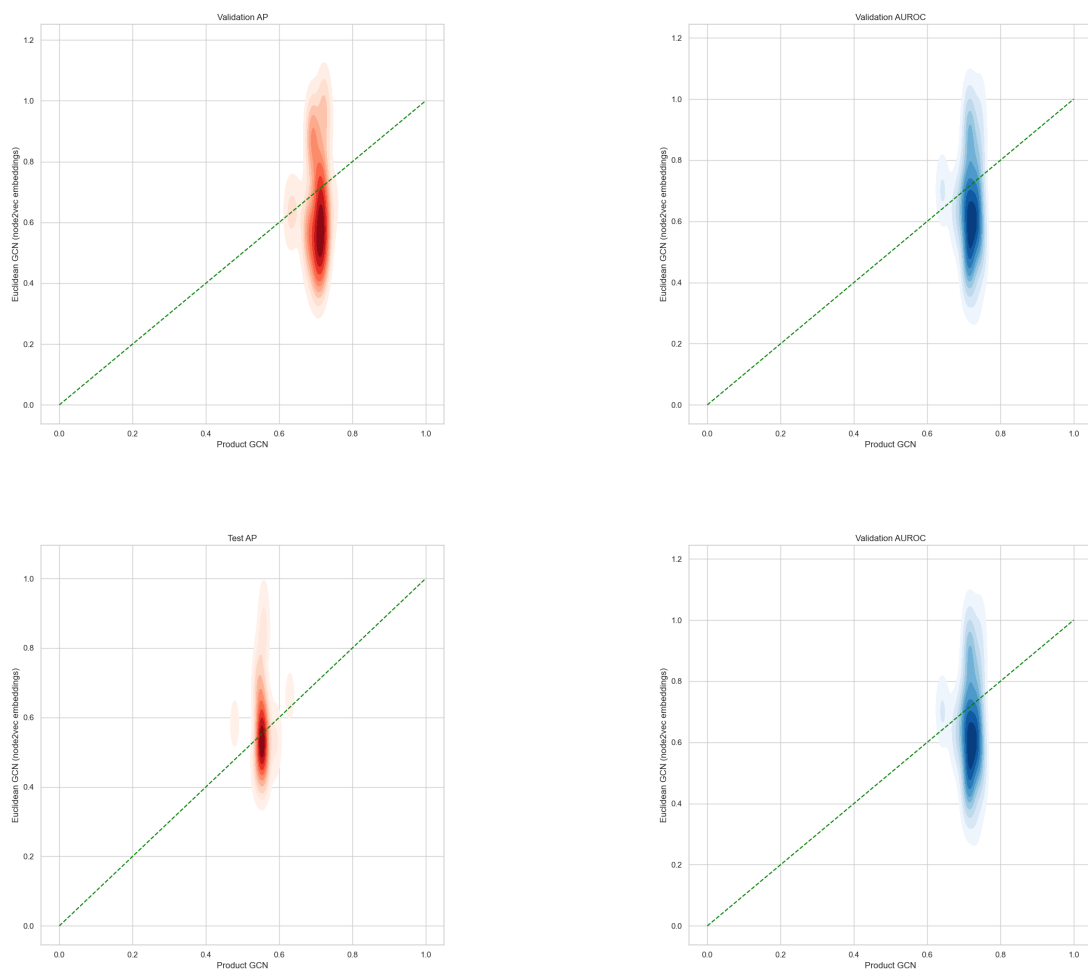


Figure 19. Comparison of Euclidean GCN initialized with pretrained node2vec embeddings and Product GCN performance on in-distribution validation set and out-of-distribution test set. Each density plot shows one of either AP or AUROC metrics taken across all graphs in the KEGG dataset.